On bifurcations of Lorenz attractors in the Lyubimov-Zaks model

Alexey Kazakov[1, a)]
National Research University Higher School of Economics,
25/12 Bolshaya Pecherskaya Ulitsa, 603155 Nizhny Novgorod, Russia

(Dated: 25 August 2021)

We provide numerical evidence for the existence of the Lorenz and Rovella (contracting Lorenz) attractors in the generalization of the Lorenz model proposed by Lyubimov and Zaks. The Lorenz attractor is robustly chaotic (pseudo-hyperbolic) in contrast to the Rovella attractor which is only measure-persistent (it exists for a set of parameter values, which is nowhere dense but has a positive Lebesgue measure). It is well known that in this model, for certain values of parameters, there exists a homoclinic butterfly (a pair of homoclinic loops) to the symmetric saddle equilibrium, which is neutral, i.e., its eigenvalues $\lambda_2 < \lambda_1 < 0 < \gamma$ are such that the saddle index $\nu = -\lambda_1/\gamma$ is equal to 1. The birth of the Lorenz attractor at this codimension-two bifurcation is established by means of numerical verification of the Shilnikov criterion. For the birth of the Rovella attractor, we propose a new criterion which is also verified numerically.

It is well-known that in the classical Lorenz and Shimizu-Morioka models, in the regions of parameters corresponding to chaotic attractors, expansion always prevails over contraction near the saddle equilibrium. This important property allows such attractors to be pseudohyperbolic, i.e., robustly chaotic in an open region of parameter values. Recall that pseudohyperbolicity implies that each orbit in the attractor has the positive maximal Lyapunov exponent, and this property persists under small perturbations[1,2]. In this paper, we consider the generalization of the Lorenz model proposed by Lyubimov and Zaks[3], in which the existence of Lorenz-like attractors of two different types was shown: attractors that contain the saddle near which expansion prevails over contraction and attractors containing the saddle near which contraction prevails over expansion. The latter attractors are called contracting Lorenz attractors or Rovella attractors because their theory was developed by Rovella[4]. Note that the Rovella attractors cannot be pseudohyperbolic, unlike the Lorenz attractors. For the example of the Lyubimov-Zaks model, we study mechanisms of the pseudohyperbolicity violation at the transition between the Lorenz attractor and the Rovella attractor. Concerning the Lorenz attractor, we give numerical evidence of its existence in this model. For the Rovella attractor, we provide a criterion of its birth from a codimension-two bifurcation. This result is similar to the well-known Shilnikov criterion[5] giving effectively verifiable conditions for the birth of the Lorenz attractor at the codimension-two bifurcation of a symmetric homoclinic butterfly to the neutral saddle (near which expansion is equal to contraction). Finally, by analysing the 1D factor map, we explain: (i) when only a region of the existence of the Lorenz attractor adjoins a codimension-2 point; (ii) when both the Lorenz attractor region and the region of the Rovella attractor existence adjoin to this bifurcation point; (iii) when only the Rovella attractor region adjoins to this point.

[a)]Electronic mail: kazakovdz@yandex.ru

I. INTRODUCTION

We study chaotic dynamics in the Lyubimov-Zaks model

$$\begin{cases} \dot{x} = \sigma(y-x) + \sigma D y(z-r) \\ \dot{y} = x(r-z) - y \\ \dot{z} = xy - bz \end{cases} \tag{1}$$

proposed in Ref. [3] as a generalization of the well-known classical Lorenz model[6]. This system describes convection in a horizontal liquid layer under the action of high-frequency vibrations. Here b, r, σ are the Lorenz model parameters, and D is a vibration parameter. In what follows, we fix

$$b = 8/3 \quad \text{and} \quad \sigma = 10$$

and study the dynamics of system (1) as a function of the parameters D and r. In the absence of vibration (when $D = 0$) it is exactly the Lorenz system. For $D \neq 0$, system (1) also exhibit chaotic attractors associated with the saddle equilibrium $O(0,0,0)$ for a vast region of parameter values (yellow-colored areas in the Lyapunov diagram, see Figure 1). Depending on the saddle index

$$\nu = -\lambda_1/\gamma$$

where $\lambda_1 < 0 < \gamma$ are the two nearest to the imaginary axis eigenvalues of the saddle O, chaotic attractors we study in system (1) belong to one of the two different types: Lorenz-like – when $\nu \in (0,1)$ and Rovella-like – when $\nu > 1$. Both types of the attractors, as well as the structure of their existence regions, are studied in this paper.

On the Lorenz attractors in system (1)**.**

We give numerical evidence for the existence of the Lorenz attractors in system (1) for an open region of parameter values. Here under the Lorenz attractor we mean a chaotic attractor of a three-dimensional flow whose Poincare map satisfies conditions of the Afraimovich-Bykov-Shilinikov (ABS) geometric model[7,8]. These conditions imply that the attractor is *pseudohyperbolic*. The latter means that, at every point of the attractor, there exist both a direction of strong contraction and a subspace, transverse to it, in which the two-dimensional volumes are expanded. The notion of pseudohyperbolicity was

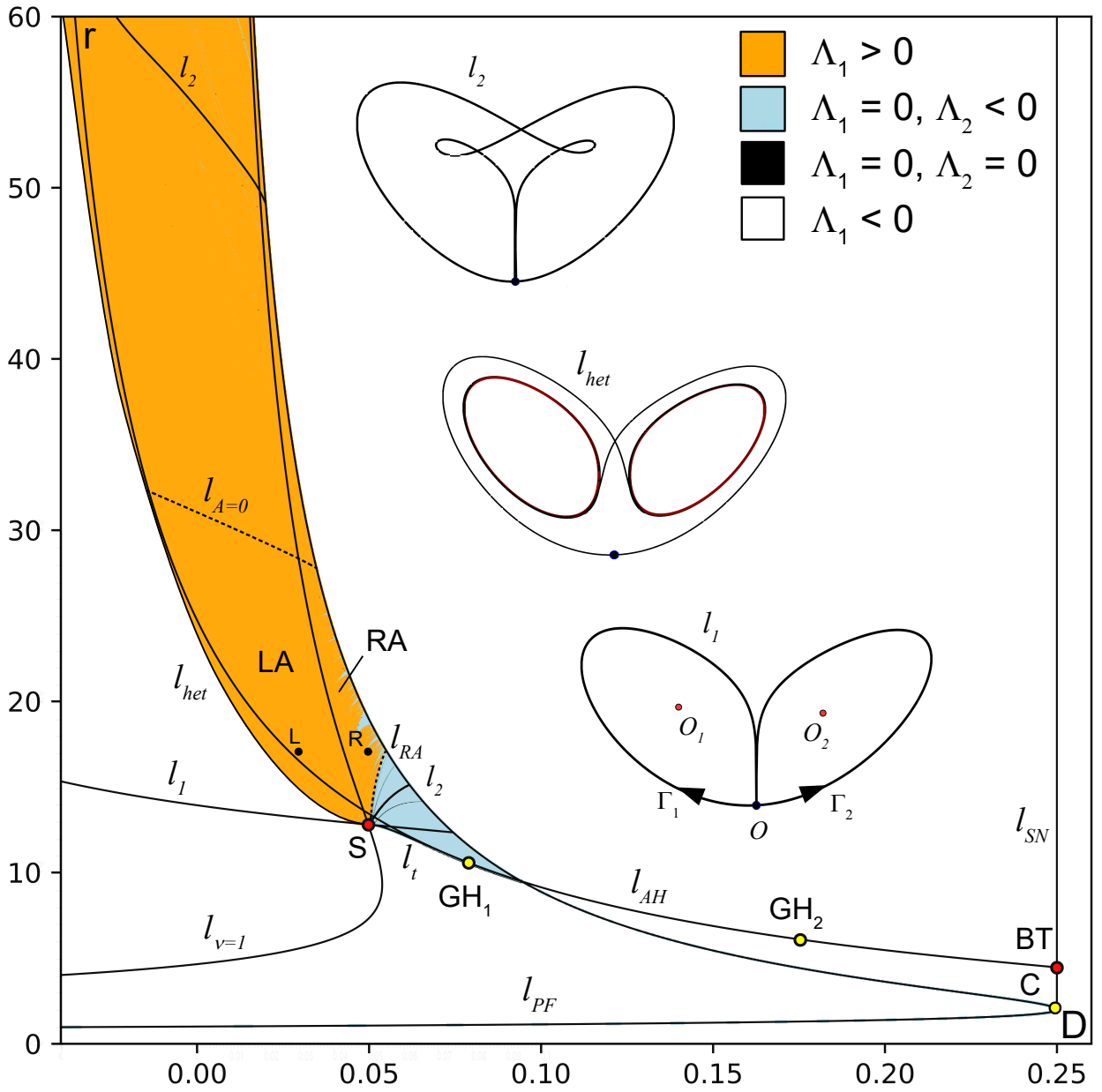

FIG. 1. Bifurcation diagram superimposed with the chart of Lyapunov exponents (see the palette in the top-right corner) on the (D, r)-parameter plane of system (1) (here $b = 8/3$ and $\sigma = 10$): l_{PF} – pitchfork bifurcation of the equilibrium O: below the codimension-2 point C this bifurcation is supercritical while above this point it is subcritical; l_{AH} – Andronov-Hopf bifurcations of the equilibriua O_1 and O_2: between the codimension-two points GH$_1$ and GH$_2$ (corresponding to the generalized Andronov-Hopf bifurcation) this bifurcation is supercritical and this bifurcation is subcritical outside this segment; l_{SN} – saddle-node bifurcation due to which O_1 merges with O_3 (by the symmetry, O_2 merges with O_4); point BT, corresponding to a Bogdanov-Takens bifurcation, divides l_{SN} onto two parts, more detailed diagram near this point is presented in Fig. 2; l_1 and l_2 – homoclinic butterfly and doubled homoclinic butterfly bifurcations, see the phase portraits with these homoclinics in the inserts. Point S of the intersection of l_1 with the neutral saddle curve $l_{v=1}$ gives the origin of the Lorenz attractor existence region LA and the Rovella attractor existence region RA. The LA-region is bounded on the left by the curve l_{het} where the unstable separatrices of O asymptotically approach the saddle limit cycles C_1 and C_2 (which are born above l_1); the RA-region is bounded from below by the limit curve l_{RA}. The curve $l_{A=0}$ corresponds to the tangency between the strongly-contracting and volume-expanding subspaces. System (1), for considered parameter values, has always negative divergence, therefore, two zero Lyapunov exponents can appear only for nonhyperbolic limit cycles (or stable equilibria with double zero eigenvalue), i.e., the chart does not contain black-colored regions, only some curves (in particular, curves $p_1, p_2, \ldots$ corresponding to pitchfork bifurcations with symmetric stable limit cycles shown in Fig. 4). Two points L and R, inside the regions LA and RA, correspond to the parameter values for which we present the detailed studies of chaotic attractors in Sections III and IV.

introduced by D. Turaev and L.P. Shilnikov[1,2], for a definition see also Refs. [9, 10] and Section III. Here we would like to emphasize that the Lorenz attractor (as well as any other pseudohyperbolic attractor) is robustly chaotic, i.e., each its orbit has positive maximal Lyapunov exponent and this property persists under small perturbations (changing parameters).

We show that, in the (D,r)-parameter plane of system (1), the region of existence of the Lorenz attractor originates from the codimension-2 point S corresponding to the homoclinic butterfly to the neutral saddle O, i.e., $\nu(O)=1$, see Fig. 1. Note that S is the intersection point of the homoclinic butterfly bifurcation curve l_1 with the neutral saddle curve $l_{\nu=1}$.

Let us clarify that by the homoclinic butterfly bifurcation we mean here the simultaneous appearance of two homoclinic orbits (loops) to the saddle equilibrium O, when both one-dimensional unstable separatrices Γ_1 and Γ_2 belong to the two-dimensional stable invariant manifold $W^s(O)$, see the right insert in Fig. 1. For generic three-dimensional systems, it is a codimension-2 bifurcation. However, system (1) is symmetric with respect to the transformation

$$x \to -x, \quad y \to -y, \quad z \to z. \tag{2}$$

due to which the appearance of one homoclinic loop to the saddle O at the origin automatically implies the appearance of the other loop, hence the homoclinic butterfly bifurcation has codimension one here.

It is well-known (see e.g. Chapter 13 in Ref. [11]) that near the point S the two-dimensional Poincaré map of the ABS model can be reduced to the one-dimensional factor map

$$X_{n+1} = (-\mu + A|X_n|^\nu + o(|X_n|^\nu))\mathrm{sign}(X_n), \tag{3}$$

where the point S corresponds to $\mu=0$ and $\nu=1$. Here μ is a separatrix splitting parameter for the symmetric butterfly, ν is the saddle index of the equilibrium, and A is the separatrix value. More precisely $|A|$ can be described as the maximal expansion, to which infnitesimal two-dimensional areas can be stretched by the system linearized along the homoclinic loop (the sign of A determines whether the orientation of the areas with the maximal expansion is changed with the propagation along the loop); more details on the definition of A can be found in Refs. [12, 13, 9].

According to the Shilnikov criterion[5], when $0<|A|<2$ at the point S, bifurcations of the corresponding system lead to the birth of the Lorenz attractor. By computing the separatrix value A in system (1) we show that the Shilnikov criterion is fulfilled, i.e., the Lorenz attractor existence region LA indeed originates from the point S.

Let us recall that in papers by A. Shilnikov[14–16], and by A. Shilnikov, L.P. Shilnikov, and D. Turaev[17], the fulfilment of this criterion was shown numerically for the Shimizu-Morioka model[18]. In Ref. [9] this fact was rigorously established by means of computer-assisted proof methods. Here we employ an indirect numerical method for computing the separatrix value. We estimate it by fitting the 1D map (3) to the 1D map generated by equations (1) near the point S, see Section III B.

On the Rovella attractor in system (1)**.**

Note that $\nu(O)>1$ to the right of the curve $l_{\nu=1}$. The corresponding Rovella-like attractors populate the region RA (see Fig. 1). Since the Rovella attractors contain the saddle O they cannot be pseudohyperbolic unlike the Lorenz attractors.

Indeed, in the case of the Lorenz attractor, the equilibrium O itself is pseudohyperbolic. Here, the strong contraction takes place along the eigenvector corresponding to λ_2, and the expansion of volumes takes place along the plane $S_{\lambda_1,\gamma}$ spanned by the eigenvectors corresponding to λ_1 and γ (here $\lambda_1+\gamma>0$, since $\nu<1$). The Rovella-like attractor is immediately not pseudohyperbolic, because areas in $S_{\lambda_1,\gamma}$ are contracted (here $\lambda_1+\gamma<0$, since $\nu>1$).

Dynamical properties of such attractors were studied in detail by A. Rovella in Ref. [4] where it was proved that this attractor is chaotic (almost all its orbits have positive maximal Lyapunov exponent) for a closed set of parameter values having a positive Lebesgue measure, see also Refs. [19–21]. We call it the *Rovella set*. These results are of great interest, because they give a new class of attractors in systems of differential equations that fit into the Benedicks-Carleson-Jacobson theory[22–24] of *measure-persistent* attractors.

A bifurcation scenario leading from the stable equilibrium O to the Rovella attractor was described in Ref. [3], see also Ref. [25]. It has been conjectured that the Rovella attractor appears via an infinite cascade of alternating homoclinic butterfly and pitchfork bifurcations accumulating to some limit curve (l_{RA} in Fig. 1).

In Section IV, we propose a conjecture (similar to the Shilnikov criterion) about the birth of the Rovella attractor at the codimension-two bifurcation corresponding to the point S. Avoiding details it can be formulated as follows:

- the Rovella set is adjacent to the point S from the side $\nu>1$ whenever $|A|>1$.

For the case $|A|>2$, with additional restrictions on the eigenvalues of the saddle equilibrium, this statement was proven in Ref. [26]. Our preliminary analysis shows that it is also true when $|A|>1$, the full proof of this fact will be given in a forthcoming paper. Also note that this conjecture can be reformulated for the asymmetric case, when the corresponding homoclinic bifurcation has codimension three.

According to the «*P or Q conjecture*» from Ref. [10], all strange attractors can be divided into two types: pseudohyperbolic attractors and quasiattractors. The notion of quasiattractors was introduced by Afraimovich and L.P. Shilnikov in Ref. [27]. When the system has a quasiattractor it either contains stable periodic orbits (POs) with very narrow absorbing domains or such orbits appear under arbitrarily small perturbations. Usually such stable periodic orbits are born at saddle-node bifurcations caused by homoclinic tangencies between invariant manifolds of saddle periodic orbits (including the Lorenz model[6] beyond the boundary of the Lorenz attractor existence[8]).

In this paper we show that the Rovella attractor is a quasiattractor of another nature. Saddle-node bifurcations, giving rise to the stable periodic orbits inside the RA-region, are caused here by the codimension-two bifurcations corresponding to the appearance of multi-round homoclinic butterflies to the neutral saddle O. Here homoclinic tangencies are absent, i.e., invariant manifolds of saddle periodic orbits intersect transversally. We show it by a check of the angles[28,29] between strongly-contracting and central-unstable subspaces.

In Section IV B, we present a detailed two-parameter analysis of bifurcations leading to the destruction of pseudohyperbolicity at the transition through the neutral saddle curve

$l_{\nu=1}$. It is known that in the existence region of the Lorenz attractor homoclinic bifurcations are dense[8]. We believe that this density persists on the curve $l_{\nu=1}$. The unfolding of each homoclinic bifurcation point on this curve gives rise to the region of stability[30]. Thus, the region RA contains infinitely many periodicity windows. Passing through these windows leads to the formation of multi-round Rovella attractors. Note that in the RA-region periodicity windows form a dense and open set, the complement to which (a nowhere dense closed set) corresponds to the mentioned above measure-persistent attractors.

On the birth of both Lorenz and Rovella attractors from the point S.

Finally, we would like to pay attention to the structure of the bifurcation diagram in system (1). Regions with chaotic dynamics originate from the point S on both sides of the curve $l_{\nu=1}$, see Fig. 1. This characteristic feature distinguished system (1) from other known 3D systems with the Lorenz attractors. In particular, in the Shimizu-Morioka model[18], where the Shilnikov criterion is also applicable[9,16], the region with chaotic attractors lies entirely on the side of the curve $l_{\nu=1}$ where the saddle equilibrium has $\nu \in (0,1)$, see Fig. 18.

Analysing the truncated factor map (3), we show that depending on the absolute value of A three cases of bifurcation diagram near the point S are possible.

1. When $0 < |A| < 1$, only a region of the existence of the Lorenz attractor adjoins to the point S, see Fig. 16a.

2. When $1 < |A| < 2$, both the Lorenz attractor region and the region of Rovella-like attractor existence adjoin to the point S, see Fig. 16b.

3. When $|A| > 2$, only the Rovella-like attractor region adjoins to the point S, see Fig. 16c.

The rest of the paper is organized as follows. In Section II, we describe bifurcations in the (D,r)-parameter plane of systems (1). In Section III, we recall main ideas of the theory of pseudohyperbolic attractors, illustrate them for the Lorenz attractors and provide the numerical evidence that, in system (1), the region with the Lorenz attractor is adjacent to the point S. In fact, we show that the Shilnikov criterion is fulfilled for this system at point S. In Section IV, we study the Rovella attractor in system (1) and bifurcations of the destruction of pseudohyperbolicity along the transition through the neutral saddle curve $l_{\nu=1}$. Also we discuss the Conjecture 1 on the birth of the Rovella attractor at bifurcations of homoclinic butterflies to a neutral saddle equilibrium. Section V is devoted to the analysis of the truncated map (3) for various values of parameter A. Using these results we explain why both regions with the Lorenz and Rovella attractors originate from the point S in system (1) unlike the Shimizu-Morioka system in which only the region with Lorenz attractors originates from such a point[9,14,16].

II. MAIN BIFURCATIONS: FROM A STABLE EQUILIBRIUM TO THE LORENZ AND ROVELLA ATTRACTORS.

The detailed bifurcation analysis of system (1) can be found in Refs. [3], [31], [32]. Let us recall some important features of the corresponding bifurcation diagram. Bifurcations curves on the (D,r)-parameter plane superimposed with the chart of Lyapunov exponents are presented in Figure 1. Most of bifurcation curves are found by means of the MatCont package[33,34]. The Lyapunov diagrams are computed using our toolkit[35]. For their calculation, at each parameter values, we take an orbit with the initial point near the origin and estimate Lyapunov exponents using the standard scheme[36]. Depending on values of Lyapunov exponents, each point in the (D,r)-parameter diagram is colored according to the palette presented in the upper-right corner of Fig. 1.

Recall that system (1) possesses the symmetry (2). It always has the symmetric equilibrium state O at the origin. Depending on parameter values, it can have two or four additional equilibrium states. On the curve l_{PF} given by the equation

$$D = \frac{R-1}{R^2},$$

the equilibrium O undergoes a pitchfork bifurcation. This curve consists of two segments separated by a point C, see Fig. 1. Below this point the pitchfork bifurcation is supercritical: O becomes saddle and a symmetric pair of stable equilibria O_1 and O_2 appears in its neighborhood when crossing the curve l_{PF} upwards. The upper segment of l_{PF} corresponds to the subcritical pitchfork bifurcation: when the upward crossing this segment, the equilibrium O becomes again stable and a symmetric pair of saddle equilibria O_3 and O_4 is born.

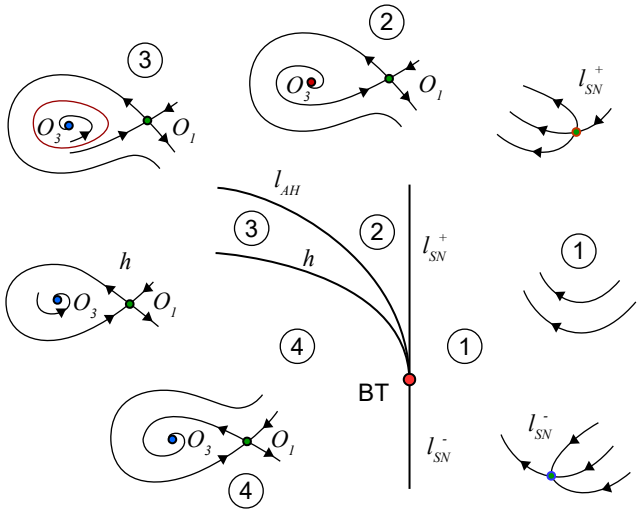

FIG. 2. Sketch of bifurcation diagram near the BT-point (see Fig. 1) corresponding to the Bogdanov-Takens bifurcation. Here, a behavior of orbits on the corresponding central two-dimensional manifold C_{BT} is shown, this invariant manifold is asymptotically stable in the case under consideration.

The equilibria O_1 and O_3 (and, by the symmetry, O_2 and O_4) collide and disappear at the saddle-node bifurcation curve

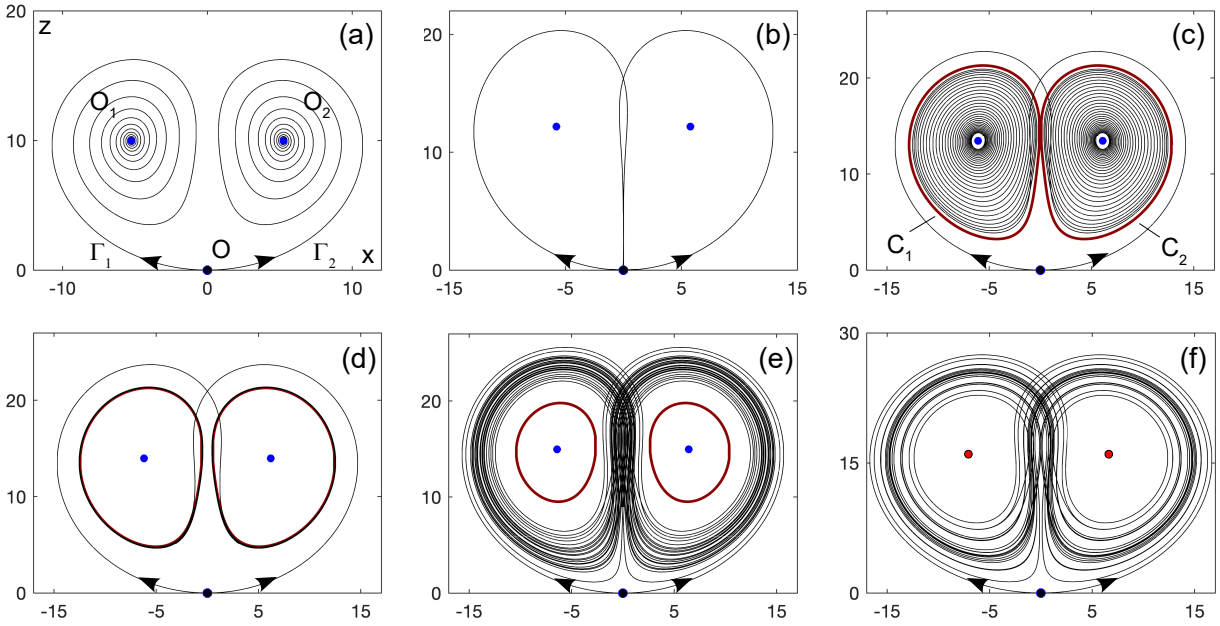

FIG. 3. Illustrations towards the scenario of the Lorenz attractor appearance in system (1). We fix $D = 0.03$ and change r: (a) the separatrices $\Gamma_1(O)$ and $\Gamma_2(O)$ tend to the stable equilibria O_1 and O_2; (b) homoclinic butterfly bifurcation on the curve l_1; (c) after this, Γ_1 (Γ_2) tends to O_2 (O_1) and a pair of saddle cycles C_1 and C_2 together with a nontrivial hyperbolic set are born; (d) on the curve l_{het}, the separatrices Γ_1 and Γ_2 lie on the stable manifold of C_2 and C_1, respectively; (e) after this, the Lorenz attractor is born; (f) on the curve l_{AH}, the equilibria O_1 and O_2 lose stability via the subcritical Andronov-Hopf bifurcation (the cycles C_1 and C_2 merge with O_1 and O_2, respectively, and these equilibria become saddles), and the Lorenz attractor remains the only attractor of the system.

l_{SN} originating from the point C and given by the equation $D = 0.25$. A point BT on this curve corresponds to the Bogdanov-Takens bifurcation, see Figure 2. Below this point the stable equilibrium O_1 (and O_2 by the symmetry) and the saddle equilibrium O_3 (and O_4 by the symmetry) are born to the left of l_{SN}. Above the BT-point all newly born equilibrium states are saddles (O_1 and O_2 with the 2D unstable manifold, while O_3 and O_4 with the 1D unstable manifold). On the curve l_{AH} originating from the BT-point the equilibrium states O_1 and O_2 undergo an Andronov-Hopf bifurcation: these equilibria are stable below this curve and they become of a saddle-focus type above l_{AH}. Below l_{AH} a homoclinic bifurcation curve (not shown in Fig. 1) with the saddle O_1 (and O_2 by the symmetry) also originates from the BT-point. We note that near the BT-point the Andronov-Hopf bifurcation is subcritical. However this bifurcation changes its type to supercritical and back at points GH_2 and GH_1 (see Fig. 1) of the generalized Andronov-Hopf bifurcation.

As was shown by Lyubimov and Zaks[3], system (1) can demonstrate two principally different scenarios of transition from simple dynamics (the stable equilibrium O) to chaotic ones. The first scenario is associated with the birth of the Lorenz attractor existing to the left of the curve $l_{v=1}$. This scenario is the same as in the classical Lorenz model[37], see Figure 3 where we fix $D = 0.03$. Here, between the curves l_{PF} and l_1 the unstable separatrices $\Gamma_1(O)$ and $\Gamma_2(O)$ tend to the stable equilibria O_1 and O_2, respectively, see Fig. 3a. On the curve l_1 homoclinic butterfly bifurcation occurs, see Fig. 3b. As a result, a pair of saddle cycles C_1 and C_2 together with a nontrivial hyperbolic invariant set are born above l_1. Also note that just after this the separatrices Γ_1 and Γ_2 tend to the equilibria O_2 and O_1, respectively, see Fig. 3c. On the curve l_{het}, the separatrices Γ_1 and Γ_2 lie on the stable manifold of the saddle cycles C_2 and C_1, respectively, see Fig. 3d, and the

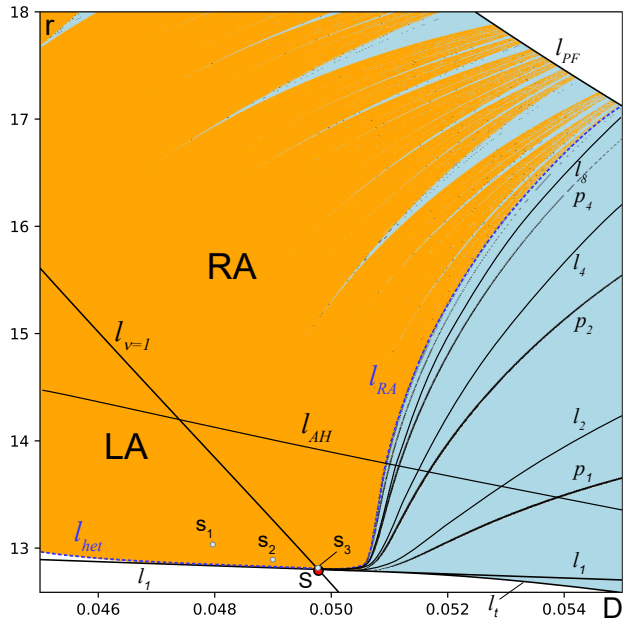

FIG. 4. Enlarged fragment of the diagram presented in Fig. 1 near the point S. Here the curves l_n ($n = 1,2,4,\ldots$) correspond to the n-round homoclinic butterfly bifurcation; and p_n ($n = 1,2,4\ldots$) correspond to the supercritical pitchfork bifurcation with a stable symmetric $(n+1)$-round cycle. Points s_1, s_2, and s_3 near S are used as "samples" for estimating the separatrix value at the point S.

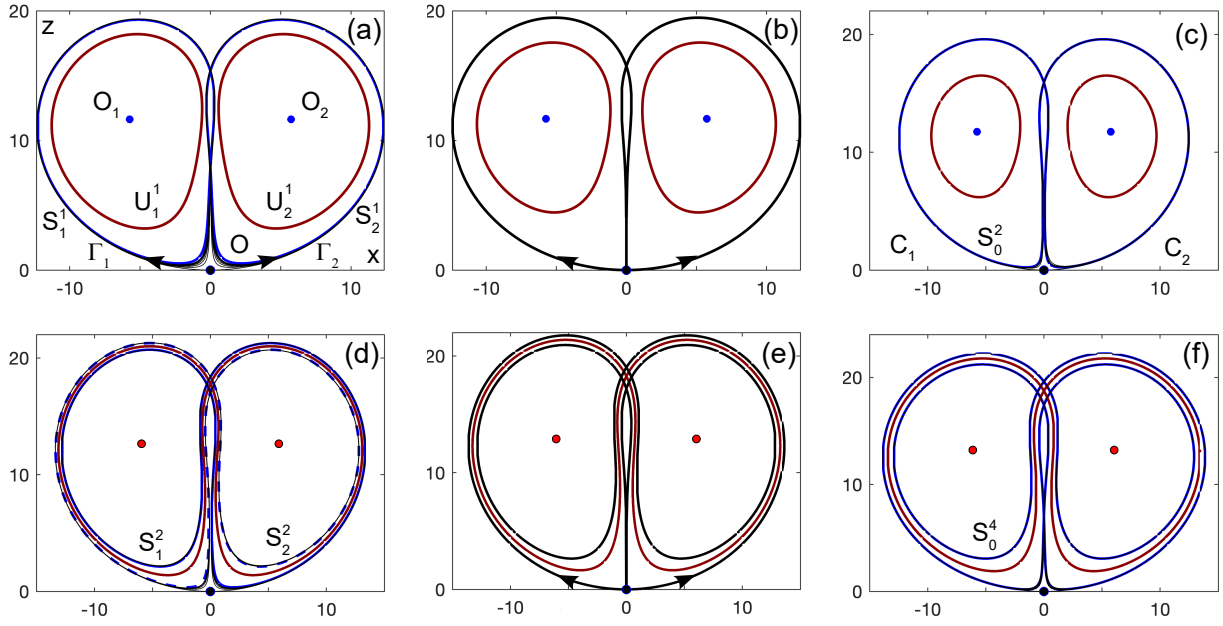

FIG. 5. Illustrations for the first steps towards the creation of the Rovella attractor in system (1). We fix $D = 0.054$ and change r: (a) the unstable separatrices $\Gamma_1(O)$ and $\Gamma_2(O)$ tend to the stable cycles S_1^1 and S_2^1 which are born together with saddle ones (U_1^1 and U_2^1) via a saddle-node bifurcation on the curve l_t; (b) S_1^1 and S_2^1 degenerate into the homoclinic butterfly on the curve l_1; (c) after this, the symmetric stable two-round cycle S_0^2 is born; (d) the pair of stable cycles S_1^2 and S_2^2 is born after the supercritical bifurcation of the cycle S_0^2; (e) the cycles S_1^2 and S_2^2 degenerate into the two-round homoclinic butterfly on the curve l_2; (f) after this, the stable four-round cycle S_0^4 is born.

Lorenz attractor is born above this curve. Note that between the curves l_{het} and l_{AH}, the Lorenz attractor coexists with the stable equilibria O_1 and O_2, see Fig. 3e. On l_{AH}, the saddle cycles C_1 and C_2 collide with O_1 and O_2 via the subcritical Andronov-Hopf bifurcation, and the Lorenz attractor remains the only attractor of the system, Fig. 3f.

The second scenario, studied in Ref. [3], leads to the birth of a Rovella-like attractor. In contrast to the above scenario, it consists of an infinite cascade of bifurcations. Let us briefly explain them. For convenience, we show an enlarged fragment of the bifurcation diagram near the point S in Figure 4. Some illustrations towards this scenario for $D = 0.054$ are shown in Figure 5. At the beginning, as in the Lorenz case, the unstable separatrices $\Gamma_1(O)$ and $\Gamma_2(O)$ tend to O_1 and O_2 (as in Fig. 3a). On the curve l_t a saddle-node bifurcation for cycles occurs and, as a result, a pair of saddle U_1^1 and stable S_1^1 cycles is born around the stable equilibrium states O_1 (by the symmetry cycles U_2^1 and S_2^1 are born around O_2). After this, the unstable separatrices of O tend to the newly born stable cycles, Fig. 5a. Note that the curve l_t originates at the point S, where the homoclinic butterfly to the neutral saddle O occurs, and terminates at the GH_1-point corresponding to the generalized Andronov-Hopf bifurcation.

On the curve l_1 the symmetric pair of stable cycles S_1^1 and S_2^1 degenerates into the homoclinic butterfly to O, Fig. 5b. As a result, above l_1 a symmetric stable two-round cycle S_0^2 is born[30], Fig. 5c. The cycle S_0^2 undergoes the supercritical pitchfork bifurcation on the curve p_1. It becomes saddle and a symmetric pair of stable two-round cycles S_1^2 and S_2^2 is born in its neighborhood, Fig. 5d (here also the subcritical Andronov-Hopf bifurcation on the curve l_{AH} occurs and the equilibria O_1 and O_2 become saddle-foci). These cycles degenerate into a two-round homoclinic butterfly on the curve l_2, Fig. 5e. Above this curve, a symmetric stable four-round cycle S_0^4 is born, Fig. 5f. It undergoes the supercritical pitchfork bifurcation on the curve p_2. Then, on the curve l_4, the newly born stable cycles S_1^4 and S_2^4 degenerate into a four-round homoclinic butterfly, and so on. This cascade of the alternating homoclinic butterfly bifurcations and pitchfork bifurcations accumulates to the limit curve l_{RA} above which a chaotic attractor is born[3].

The same as Feigenbaum-like attractors, occurring via the cascade of period-doubling bifurcations, this attractor, just after its birth, has lacunae containing the symmetric 2^n-round saddle cycles (appearing as a result of the pitchfork bifurcations with the cycles $S_0^{2^n}$) which do not belong to the attractor. With a further increase in r, these cycles, in the reverse order, start to be captured by the attractor via heteroclinic bifurcations, which occur when the unstable separatrices Γ_1 and Γ_2 lie on stable manifold of these symmetric saddle cycles. As was shown by Rovella[4], such heteroclinic bifurcations (under some additional restrictions on the eigenvalues of the equilibrium O) imply the measure-persistence of the corresponding attractors.

Rovella-like attractors populate the region RA, see Figs. 1 and 4. The curves l_{RA}, l_{PF}, $l_{v=1}$, and $l_{A=0}$ form the boundaries of this region.

At the end of this section, we would like to note that the Rovella attractor can appear immediately (from the Lorenz attractor) when passing through the curve $l_{v=1}$.

III. ON PSEUDOHYPERBOLICITY AND THE LORENZ ATTRACTORS IN SYSTEM (1)

In the Lyapunov diagrams presented in Figs. 1 and 4, one can see that the region LA of the Lorenz attractor existence is free of stability (periodicity) windows, in contrast to the region RA where infinitely many such windows complement a nowhere dense set of parameter values with chaotic attractors. Such organization of the Lyapunov diagrams in LA is typical for pseudohyperbolic attractors, to the class of which the Lorenz attractors belong. Let us recall the definition of pseudohyperbolicity given in Refs. [9], [10].

Definition 1 *A flow $\mathscr{F}_t$ in $\mathbb{R}^n$ is called pseudohyperbolic in a strictly forward-invariant domain $\mathscr{A} \in \mathbb{R}^n$ (i.e., $\mathscr{F}_t(\mathscr{A}) \subset \mathscr{A}$ for $t > 0$) if it possesses the following properties:*

(A) *For each point x of $\mathscr{A}$ there exist two continuously dependent on x linear subspaces, $E_1(x)$ with $\dim E_1 = k$ and $E_2(x)$ with $\dim E_2 = n-k$, which are invariant with respect to the linearized flow DF:*

$$DF_t E_1(x) = E_1(F_t(x)), \qquad DF_t E_2(x) = E_2(F_t(x)),$$

for all $t \geq 0$ and all $x \in \mathscr{A}$.

(B) *The splitting to E_1 and E_2 is dominated, i.e., there exist constants $C_1 > 0$ and $\beta > 0$ such that*

$$\|DF_t(x)|_{E_2}\| \cdot \|(DF_t(x)|_{E_1})^{-1}\| \leq C_1 e^{-\beta t}$$

for all $t \geq 0$ and all $x \in \mathscr{A}$. (This condition means that any possible contraction in $E_1(x)$ is uniformly weaker then any contraction in $E_2(x)$, and any expansion in $E_1(x)$ is uniformly stronger than any possible expansion in $E_2(x)$).

(C) *The differential DF restricted to E_1 exponentially expands all k-dimensional volumes, i.e., there exist constants $C_2 > 0$ and $\sigma > 0$ such that*

$$det(DF_t(x)|_{E_1}) \geq C_2 e^{\sigma t}$$

for all $t \geq 0$ and all $x \in \mathscr{A}$.

Now, following Ref. [9], we can consider the Lorenz attractor of the Afraimovich-Bykov-Shilnikov model as the attractor of a pseudohyperbolic flow with $\dim(E_1) = 2$.

In this paper, we deal only with the three-dimensional system (1). In this case, $\dim(E_2) = 1$ and, since all vectors are contracted in E_2, it is convenient to use denotations E^{cu} and E^{ss} instead of E_1 and E_2, respectively.

In Ref. [10] (see also [38]) it was shown how to check the conditions of Def. 1 numerically. For verification of the conditions (B) and (C), one should calculate the spectrum of Lyapunov exponents $\Lambda_1 \geq \Lambda_2 \geq \Lambda_3$:

- condition (B) equals to $\Lambda_2 > \Lambda_3$;
- condition (C) equals to $\Lambda_1 + \Lambda_2 > 0$.

Note that these conditions should be satisfied for all orbits in the attractor. An efficient method to verify them is to take only one sufficiently long "representative" orbit in the attractor, cut it into many quite short pieces and, then, check conditions (B) and (C) for each such piece[10,38]. For the attractor presented in Fig. 3f, some results of the corresponding Lyapunov analysis are shown in Figure 6 (top row). For this experiment, we take an orbit returning 10^5 times to the cross-section $z = 16$, cut it into $2 \cdot 10^4$ or 10^4 pieces of length $T_s = 5$ or $T_s = 10$, respectively, and compute, for both cases, histograms of finite-time Lyapunov exponents[39,40] Λ_2 (Fig. 6a), Λ_3 (Fig. 6b), and $\Lambda_1 + \Lambda_2$ (Fig. 6c). Histograms for $T_s = 5$ are colored in blue and histograms for $T_s = 10$ – in orange. Condition (B) is obviously satisfied since the always-negative exponent Λ_3 is clearly separated from the near-zero exponent Λ_2. Fig. 6c shows the fulfilment of condition (C).

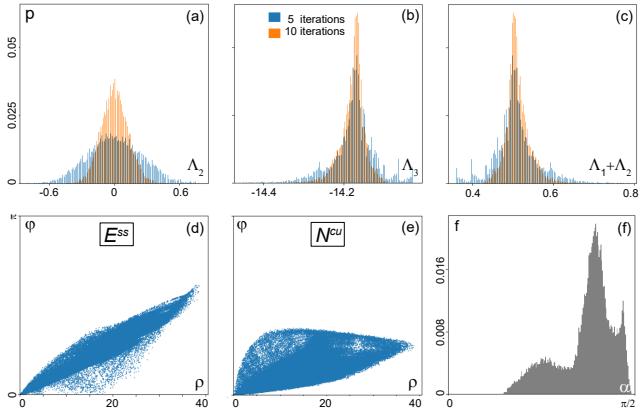

FIG. 6. Results of pseudohyperbolicity verification for the attractor of system (1) presented in Fig. 3f (point L: $(D,r) = (0.03,17)$ in Fig. 1): (a), (b), (c) histograms of finite-time Lyapunov exponents Λ_2, Λ_3, as well as the sum $\Lambda_1 + \Lambda_2$, which are computed by an orbit returning 10^5 times to the cross-section $z = 16$ cut into $2 \cdot 10^4$ (blue-colored bins) and 10^4 pieces (orange-colored bins) of length 5 and 10, respectively; (d), (e) continuity diagrams for E^{ss} and N^{cu}, (f) histogram of the angles between the subspaces E^{ss} and E^{cu}. These graphs show that all pseudohyperbolicity conditions of Def. 1 are fulfilled, i.e., the attractor is pseudohyperbolic.

Verification of condition (A) is much more delicate problem. It is based on calculation of the Lyapunov co-variant vectors[28,29] and construction (using these vectors) of either the so-called E^{ss}- and E^{cu}-continuity diagrams, as was proposed in Ref. [10], or angles between the subspaces E^{ss} and E^{cu}, as was done in Refs. [40] and [38]. The latter method is based on the fact that the E^{ss}- and E^{cu}-continuity condition (A) of Def. 1 implies to the absence of tangencies between these subspaces[38]. Results of both methods are presented in Figure 6d–f. The corresponding graphs show the continuity of E^{ss} (see Fig. 6d) and E^{cu} (see Fig. 6e, where the graph for normal vectors N^{cu} is presented), as well as the absence of zero angles between E^{ss} and E^{cu} along a sufficiently long ($T = 10^6$) orbit (see Fig. 6f). In general, these results confirm the fulfilment of condition (A) and, thus, pseudohyperbolicity of the attractor presented in Fig. 3f.

A. Shilnikov criterion

We also propose an alternative method which not only helps to confirm pseudohyperbolicity of observed attractors but also allows to establish the existence of the Lorenz attractor in system (1) for an open set of parameter values. This method is based on the verification of the Shilnikov criterion[5]. A detailed description of this criterion can be found in book [11], see also recent papers [9] and [41]. Let us recall it.

Consider a system of differential equation in $\mathbb{R}^n$ possessing a saddle equilibrium O with eigenvalues $\gamma, \lambda_1, \lambda_2, \ldots, \lambda_{n-1}$ such that:

$$\gamma > 0 > \lambda_1 > \mathrm{Re}(\lambda_i) \quad i \geq 2.$$

Assume that this system is invariant with respect to a symmetry $\mathbb{S}$, such that O is a symmetric equilibrium ($\mathbb{S}\,O = O$) and the eigenvectors V_γ and V_{λ_1} corresponding to the eigenvalues γ and λ_1 are $\mathbb{S}$-invariant: $\mathbb{S}\,V_\gamma = -V_\gamma$ and $\mathbb{S}\,V_{\lambda_1} = V_{\lambda_1}$. We also assume that this symmetry implies a symmetry of two unstable separatrices Γ_1 and Γ_2 touching the eigenvector V_γ at point O, i.e., $\mathbb{S}\,\Gamma_1 = \Gamma_2$ and $\mathbb{S}\,\Gamma_2 = \Gamma_1$. Further assume that the following three conditions for the system are fulfilled:

1. both unstable separatrices Γ_1 and Γ_2 return to O at $t \to +\infty$ touching the eigenvector V_{λ_1}, i.e., a homoclinic butterfly bifurcation to O is created;
2. the saddle index ν of O is equal to one, i.e., $\nu = -\lambda_1/\gamma = 1$;
3. the separatrix value A satisfies the condition

$$0 < |A| < 2. \tag{4}$$

According to L.P. Shilnikov[5], bifurcations of such system lead to the birth of the Lorenz attractor.

It is worth noting that in the class of $\mathbb{S}$-symmetric systems under consideration, conditions 1 and 2 correspond to a codimension-2 bifurcation. Thus, if to embed such a system into a two-parameter family $F_{\mu,\nu}$ of systems for which varying μ and ν we can independently split the homoclinic butterfly and change the saddle index near 1 we can formulate the Shilnikov criterion more precisely[5,9]:

Theorem 1 (L.P. Shilnikov[5]) *If condition* (4) *is fulfilled in the codimension-2 point (when system $F_{\mu,\nu}$ has a homoclinic butterfly with a neutral saddle), then in the (μ,ν)-parameter plane there exists an open region with the Lorenz attractor of the Afraimovich-Bykov-Shilnikov model and the point $(\mu,\nu) = (0,1)$ belongs to its boundary.*

The proof of this theorem can be found in Ref. [42].[43]

Concerning system (1), the homoclinic butterfly to the neutral saddle O occurs here at the point S, where the curve of homoclinic butterfly bifurcation l_1 intersects with the neutral saddle curve $l_{\nu=1}$ (see Figs. 1 and 4). In order to apply the Shilnikov criterion it remains only to compute the separatrix value A at this point.

Note, in such a way the existence of the Lorenz attractor was proven in Ref. [9] for the Shimizu-Morioka model. The separatrix value A was computed for the homoclinic loop by a 3D flow exactly in the codimension-2 bifurcation point by means of computer-assisted proof methods. We propose another method for estimating the separatrix value A.

B. Separatrix value from the numerically obtained 1D maps

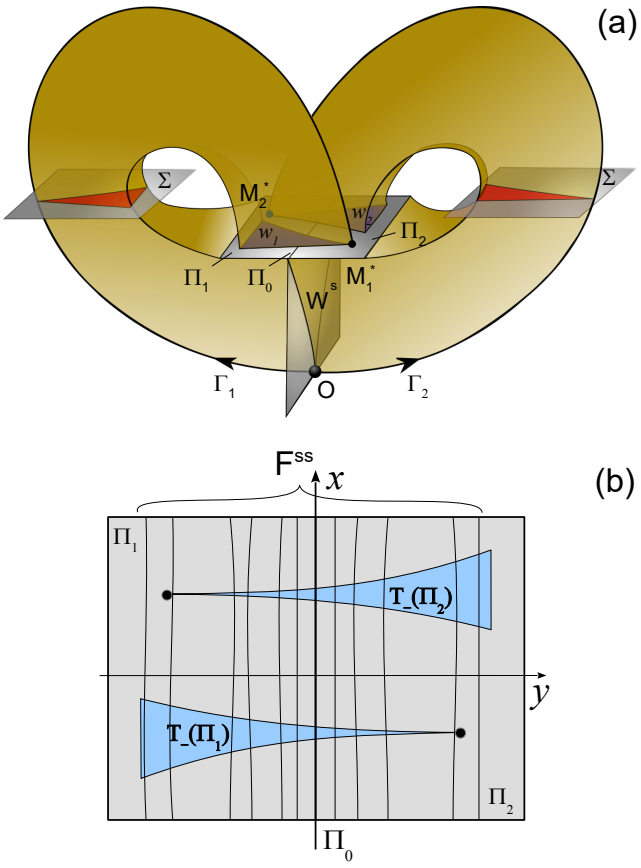

FIG. 7. (a) An illustration towards the geometric Afraimovich-Bykov-Shilnikov model; (b) two-dimensional Poincaré map on the cross-section Π.

The approach for studying the Lorenz attractor, proposed by Afraimovich, Bykov, and L.P. Shilnikov[7,8], is to consider (instead of the original system of differential equations) a geometric model – 2D singular-hyperbolic discontinuous map which is, in a sense, a generalization of Poincaré map near the separatrix loop to a saddle equilibrium. The term singular-hyperbolic stresses a fact that the map has a discontinuity line. Figure 7 illustrates main ideas of this approach. Here, a peace of horizontal plane is a cross-section Π taken near the saddle equilibrium O, transversal to its stable invariant manifold $W^s(O)$. The unstable separatrices $\Gamma_1(O)$ and $\Gamma_2(O)$ intersect the cross-section Π at points M_1^* and M_2^*, respectively. Note that this cross-section is separated by a line $\Pi_0 = \Pi \cap W^s(O)$ onto two parts: Π_1 and Π_2. All orbits starting in Π return to this cross-section in a finite time except for those belonging to Π_0 (they tend to O when $t \to +\infty$). By continuity, the Poincaré map T_- of the cross-section Π can be defined as it is schemat-

ically shown in Fig. 7a: a blue-colored wedge $w_1(w_2)$ with a tip at point $M_1^*(M_2^*)$ is an image of $\Pi_1(\Pi_2)$, i.e., $w_1 = T_-(\Pi_1)$ $(w_2 = T_-(\Pi_2))$, and w_1 and w_2 lie entirely in Π.

According to Afraimovich, Bykov, and L.P. Shilnikov[7,8] when the map T_- satisfies certain conditions (see, conditions (*) in Ref. [7] or condition (1.1) in Ref. [8]) it is singular hyperbolic. Moreover, in this case a strong stable invariant foliation F^{ss} exists on Π. This foliation contains the line Π_0 as a leaf and also all its preimages which densely fill the cross-section Π.[8] A schematic representation of the action of T_- is shown in Figure 7b. The existence of the foliation F^{ss} allows to factorize map T_- over the leaves of this foliation. It is important to note that, near the codimension-two point S, the resulting 1D factor map is exactly the map (3).[11]

For numerical studies, it is also convenient to consider an analogous 2D Poincaré map T_+ and its 1D factor map on a two-component cross-section Σ into which orbits enter from bottom to top, see Fig. 7a (it can be the same plane Π, however another its part, where only upward crossings are observed). One can show (analyzing the 2D Poincaré map on Σ) that the corresponding truncated factor map has the following form

$$X_{n+1} = \mu_\Sigma - A|X_n - s|^\nu. \qquad (5)$$

Here ν and A are the same parameters (saddle index and separatrix value) as in map (3), $s > 0$ represents a positive preimage of the discontinuity point on Σ, μ_Σ is the image of the unstable separatrix on this section. Note that the difference $(\mu_\Sigma - s)$ corresponds to the value of splitting for the homoclinic butterfly.

For the attractor presented in Fig. 3f, both types of the 2D Poincare maps $T_\pm : (x_n, y_n) \to (x_{n+1}, y_{n+1})$ are shown in Figure 8a. Here we take a plane $z = r - 1 = 16$ as the cross-section. A pair of blue-colored clouds of points in the middle of this graph corresponds to the intersections of Γ_1 with the cross-section Π (images of map T_-), while a pair of red-colored clouds C_l and C_r corresponds to the intersections with Σ (images of map T_+).

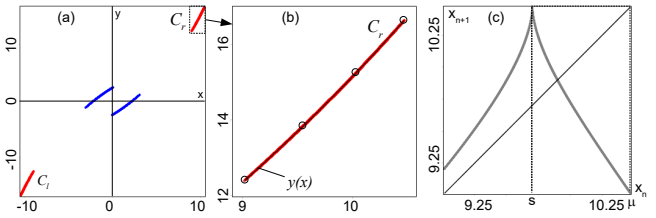

FIG. 8. (a) Poincaré map on the cross-section $z = 16$ for the attractor shown in Fig. 3f, blue (red) points correspond to 10^5 intersections of the separatrix Γ_1 moving downwards (upwards); (b) an enlarged fragment of this map near the cloud of points C_r superimposed with the Lagrange polynomial $y(x)$ constructed by four points: two points on the left (x_{min}, y_{min}) and right (x_{max}, y_{max}) edges of C_r and two middle points; (c) 1D first return map $x_{n+1} = T(x_n, y(x_n))$ reconstructed by 10000 points on the regular lattice within the segment $[x_{min}, x_{max}]$.

For a rigorous computing the 1D factor map from this 2D map, it is necessary to know the strong stable foliation F^{ss}. Such foliation can be computed as an intersection of a large piece of $W^s(O)$ with the cross-section Π or Σ (it does not matter which one)[44–46]. For a sufficiently good approximation of the 1D map, we suggest another simple procedure based on the fact that, due to the strong contraction, points of the intersection of the Lorenz attractor with the cross-section seem to lie on 1D curves, see Fig. 8a. First, we take one of such "curves", namely C_r, and parameterize it with the Lagrange polynomial $y(x)$ using four points: two points on the left (x_{min}, y_{min}) and right (x_{max}, y_{max}) edges of C_r and two in the middle (Fig. 8b). Then, we compute the corresponding 1D first return map $x_{n+1} = T(x_n, y(x_n))$ using 10000 points taken on the regular lattice within the segment $[x_{min}, x_{max}]$. Finally, we plot the resulting points $(x_n, |x_{n+1}|)$ on the graph, see Fig. 8c. Note that we take absolute values of x_{n+1} for the representativeness of the map, since the images of points lying on different sides of the discontinuity line (where $W^s(O)$ intersects with Σ for the first time) have opposite signs.

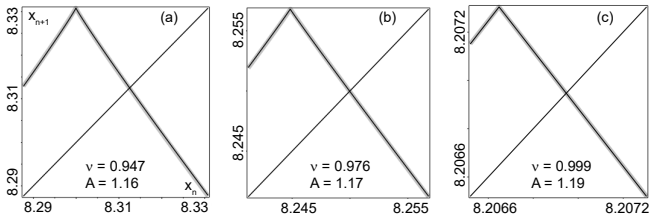

FIG. 9. Factor map (5) (black-colored line) superimposed with numerically obtained 1D maps (gray-colored line) at the points (a) s_1: $(D, r) = (0.048, 13)$; (b) s_2: $(D, r) = (0.049, 12.88)$; (c) s_3: $(D, r) = (0.04975, 12.805)$ approaching the point S: $(D, r) = (0.0497, 12.8)$.

Note that the numerically obtained 1D map presented in Fig. 8c has the same form as map (5). A natural question arises here. How to select parameters ν, μ_Σ, s, and A of the last map in order to get the best fitting with the numerically obtained map? Parameter ν is simply computed as the saddle index of equilibrium O. Parameters s and μ_Σ are found from the numerically obtained 1D map: s – the preimage of the discontinuity point, μ_Σ – its image. The last parameter A is selected to provide the best match (by means of the least square method) between the map (5) and the numerically obtained 1D map. Note that the numerically obtained map cannot be well approximated by map (5) when the parameters (D, r) are chosen sufficiently far from the point S (in this case, term $O(|X - s|^{\nu_2})$, where $\nu_2 = \min(2\nu, -\lambda_2/\gamma)$ are not longer small). However, the closer to S we take a point, the better map (5) can be fitted to the numerically obtained one. Figure 9 confirms this fact. This figure shows (in gray color) a series of 1D maps computed by the corresponding 2D Poincaré maps at points s_1, s_2, and s_3 taken in the (D, r)-parameter plane near the point S (dist(s_1, S) = 0.2, dist(s_2, S) = 0.079, and dist(s_3, S) = 0.004) superimposed with the reconstructed 1D maps (5) (in black color). Parameters of the corresponding reconstructed 1D maps are as follows:

s_1 : $\nu = 0.947, \mu_\Sigma = 8.3308, s = 8.2999$, and $A = 1.16$;

s_2 : $\nu = 0.976, \mu_\Sigma = 8.2568, s = 8.2448$, and $A = 1.17$;

s_3 : $\nu = 0.999, \mu_\Sigma = 8.2073, s = 8.2066$, and $A = 1.19$.

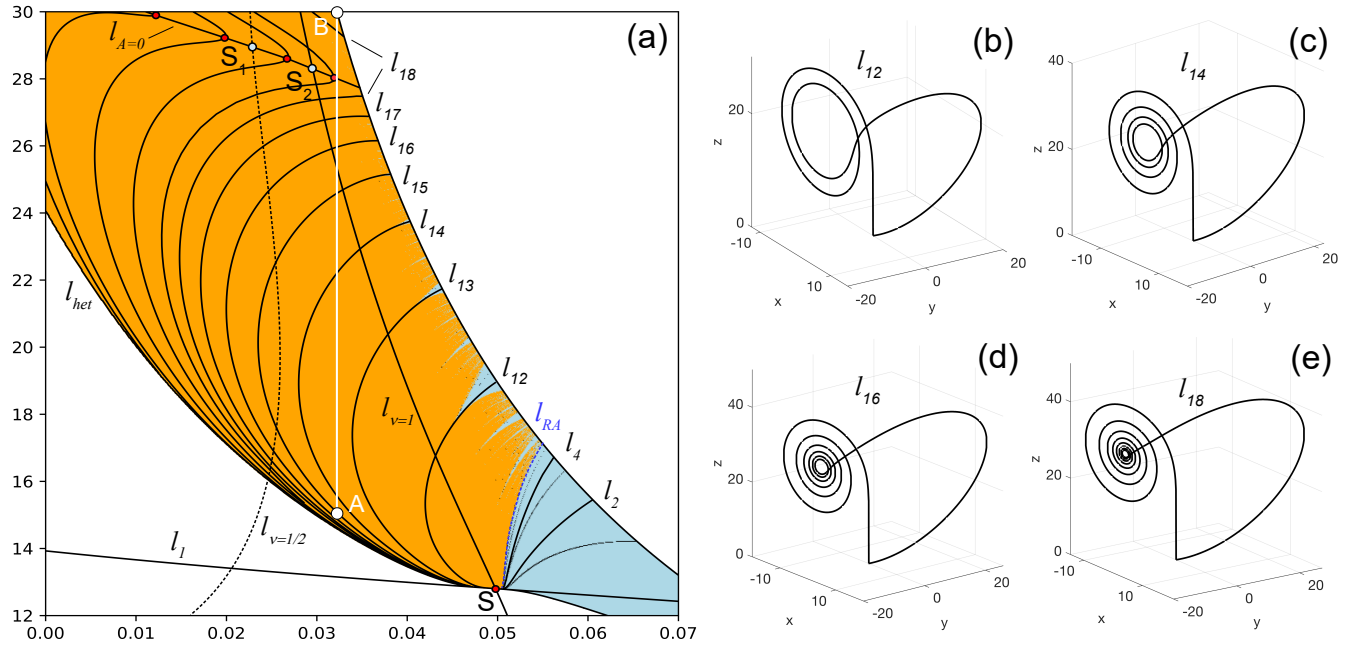

FIG. 10. (a) Some bifurcation curves superimposed with the Lyapunov diagram. $l_{\nu=1/2}$ – the curve where the saddle index $\nu(O) = 1/2$, $l_{A=0}$ – the curve on which the first tangency between E^{ss} and E^{cu} occurs, l_{1n}– homoclinic bifurcation curves: 1 and n mean the number of turns which the unstable separatrix Γ_2 makes around the equilibria O_1 and O_2, respectively. (b)–(e) Some homoclinic loops for even $n \in \{2,4,6,8\}$.

Thus, we see that the saddle index ν indeed approaches 1, the distance $\mu_\Sigma - s$ (separatrix splitting value) tends to zero, and $A \approx 1.19$. This value gives a good approximation for the separatrix value of system (1) at the point S.

C. Vanishing A: violation of pseudohyperbolicity and non-orientable Lorenz attractors

The upper boundary of the LA-region of the classical Lorenz attractor existence is associated with the curve $l_{A=0}$ on which the strong-stable E^{ss} and central-unstable E^{cu} subspaces intersect nontransversely. For the Lorenz system this curve was found by Bykov and A. Shilnikov[47,48] (see also Refs. [49] and [46]) by means of the 1D map analysis. Below the curve $l_{A=0}$, the corresponding 1D map has two branches without zero derivatives (see. e.g. Fig. 8c). The right branch gets zero derivative on this curve. Further evolution of the 1D map above $l_{A=0}$ results in the formation of the characteristic hook (bend) at rightmost segment of this map (see e.g. Fig. 11d for illustration). Note that in system (1) the curve $l_{A=0}$ consists of two parts divided by the point S_1 in which $\nu(O) = 1/2$, see Figure 10a.

Above the first part of this curve, where $0 < \nu < 1/2$, the strong stable foliation F^{ss} is violated, the subspaces E^{ss} and E^{cu} no longer depend continuously on a point, and the attractor becomes a *quasiattractor* of Lorenz type. Figures 11a–c illustrate this fact for an attractor taken at $(D,r) = (0.02, 30)$. The corresponding 1D map (with the hook) is shown in Figure 11d.

The second part of the curve $l_{A=0}$, where $1/2 < \nu < 1$, does not form a boundary of the region of (pseudohyperbolic) Lorenz attractor existence[16]: stable periodic orbits exist below this curve while non-orientable Lorenz attractors[8] popu-

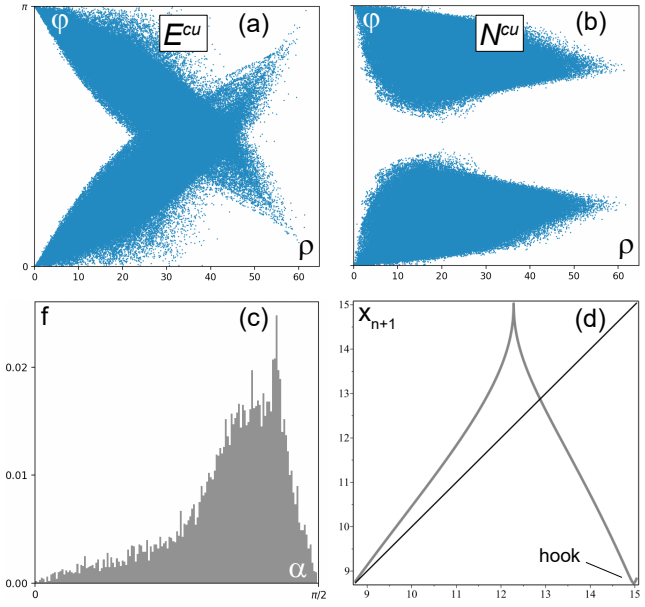

FIG. 11. Results of pseudohyperbolicity verification for the attractor of system (1) taken at $(D,r) = (0.02, 30)$: (a), (b) continuity diagrams for E^{ss} and N^{cu}, (c) histogram of angles between the subspaces E^{ss} and E^{cu}, (d) 1D map with the hook on the right branch. These experiments confirm the absence of stable foliation, i.e., we observe a Lorenz quasiattractor for these parameter values.

lating the so-called *Shilnikov flames* appear above it[16,50,51]. It is important to note that non-orientable Lorenz attractors can be pseudohyperbolic. Thus, robustly chaotic attractors exist also above the second part of $l_{A=0}$. For the Shimizu-Morioka model pseudohyperbolicity of such attractors was established in Ref. [38]. Questions related to the study of dynamics in the parameter region above this curve and non-orientable Lorenz attractors will be considered in forthcoming papers.

Finally in this Section we would like to note that the curve $l_{A=0}$ intersects (multi-round) homoclinic bifurcation curves at the so-called *inclination flip* points. In such a point the separatrix value A of the corresponding homoclinic loop vanishes and the two-dimensional stable manifold $W^s(O)$ along the loop changes orientation: it is an annulus below $l_{A=0}$ and a Möbius band – above this curve. Some (multi-round) homoclinic bifurcation curves l_{1n} are presented in Figure 10a. Here 1 and n mean the number of turns which the unstable separatrix Γ_1 makes around the equilibrium O_2 and O_1, respectively (symmetrically for Γ_2). Note that n tends to infinity when we approach the curve l_{het} where the unstable separatrices lie on the stable manifold of the saddle cycles. Homoclinic loops on the curves l_{1n} for $n \in \{2,4,6,8\}$ are shown in Figure 10b–e.

IV. ON THE ROVELLA ATTRACTOR

It is interesting to note that the continuity condition (A) of Def. 1 is preserved to the right of the curve $l_{v=1}$, in the region RA. Figure 12 shows the results of pseudohyperbolicity verification of an attractor at the point

$$R : (D,r) = (0.05, 17) \qquad (6)$$

in this region (see Fig. 1).

The E^{ss}– and N^{cu}– continuity diagrams (Figs. 12a,b), as well as the histogram of angles between the E^{ss} and E^{cu} subspaces (Fig. 12c), illustrate that both these subspaces depend continuously on a point in the attractor and there are no tangencies between them. Moreover, this property is preserved after small perturbation (changes in parameters).

Figure 13 shows the dependency of minimal angle between E^{ss} and E^{cu} on the parameter r along a pathway AB (shown in Fig. 10a): $D = 0.032, r \in [15,30]$ crossing the curves $l_{v=1}$ and $l_{A=0}$. It is clearly seen from this figure that the minimal angle is separated from zero up to the intersection of AB with the curve $l_{A=0}$ (at $r = r_{A=0} \approx 28$) where the minimal angle vanishes, and the tangency between E^{ss} and E^{cu} appears.

It is worth noting that the dominated-splitting condition (B) of Def. 1 for the attractor at point R is also preserved, see Figs. 12d,e confirming that $\Lambda_2 > \Lambda_3$ for all orbits in the attractor. Nevertheless, this attractor *cannot be pseudohyperbolic* since the volume-expanding condition (C) of Def. 1 is violated for some orbits, see Figs. 12f demonstrating that $\Lambda_1 + \Lambda_2$ can be negative.

Figure 14 shows a 2D Poincaré map and the corresponding first return 1D map for the attractor observed at point R. Note that the 2D Poincaré map for this attractor looks like for the Lorenz attractor, cf. Fig. 8a and Fig. 14a, while the 1D map (Fig. 14b) reveals the fundamental difference between these

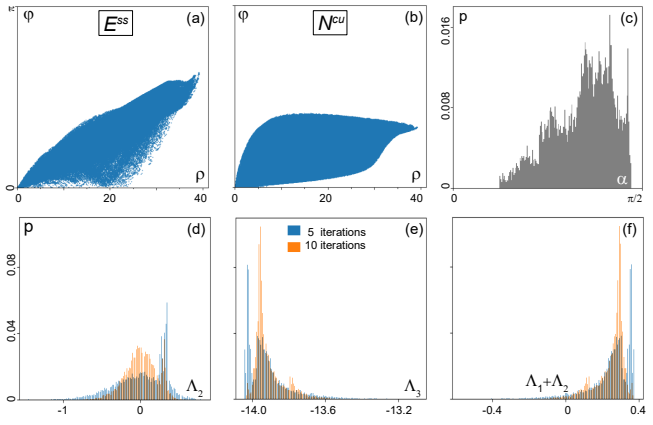

FIG. 12. Results of pseudohyperbolicity verification for the attractor of system (1) taken at $D = 0.05, r = 17$ (the point R in Fig. 1): (a), (b) continuity diagrams for E^{ss} and N^{cu}, (c) histogram of the angles between the subspaces E^{ss} and E^{cu}; (d), (e), (f) histograms of Lyapunov exponents Λ_2, Λ_3, and $\Lambda_1 + \Lambda_2$, which are computed by an orbit making 10^5 returns to the cross-section $z = 16$ cut into $2 \cdot 10^4$ (blue-colored bins) and 10^4 (orange-colored bins) pieces of length 5 and 10, respectively. From Fig. (f) one can see the violation of volume-expanding condition, i.e., the attractor cannot be pseudohyperbolic despite the preservation of continuity condition (A) of Def. 1.

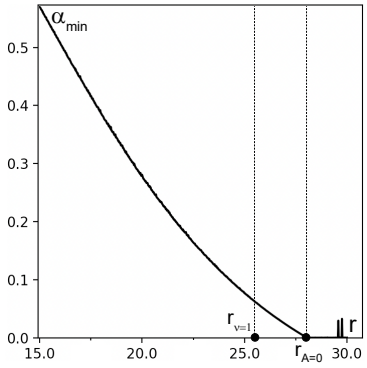

FIG. 13. Graph of dependency of the minimal angles between the subspaces E^{ss} and E^{cu} along the pathway AB: $D = 0.032, r \in [15,30]$. The minimal angle vanishes when crossing the curve $l_{A=0}$ (at $r = r_{A=0} \approx 28$). For this experiment for each value of parameter r we take an orbit of length $T = 10^5$.

attractors. The zero derivative prevents pseudohyperbolicity of the Rovella attractor.

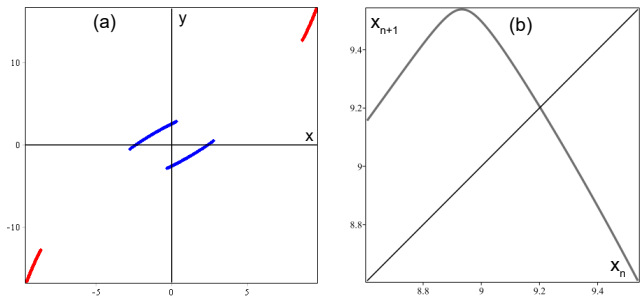

FIG. 14. (a) 2D Poincaré map on the cross-section $z = 16$ and (b) 1D first return map for the Rovella attractor observed at the point R.

The absence of pseudohyperbolicity for the Rovella attractor is in a good agreement with what is observed in the Lyapunov diagrams (Figs. 1, 4, 10) showing that, in the RA-domain, regions with chaotic attractors alternate with periodicity windows. As for any quasiattractor, after an arbitrarily small perturbation of these attractors (change in parameters) one can observe a stable periodic orbit. Nevertheless, regions with such chaotic attractors have positive Lebesgue measure in a two-parameter space (see Ref. [4] and Sec. IV A for more detail). This result is similar to the results by Benedicks, Carleson, and Jacobson[22–24] on measure-persistence of chaotic attractors in the 2D Hénon map.

A. Shilnikov-like criterion for the birth of Rovella attractor

Analyzing the truncated 1D map (3) at $A = 1.5$, Lyubimov and Zaks[3] showed that the region RA originates from the codimension-two point $(\mu,\nu) = (0,1)$ corresponding to the homoclinic butterfly bifurcation with a neutral saddle. This result can be generalized into a Shilnikov-like criterion for the birth of the Rovella attractor. The preliminary analysis shows that if we replace condition (4) with the condition

$$|A| > 1 \tag{7}$$

and add the following condition on the so-called *second saddle index* $\chi = -\lambda_2/\gamma$:

$$\chi > 2, \tag{8}$$

while keeping the remaining conditions from Sec. III A unchanged, then bifurcations of such a system lead to the birth of the Rovella attractor. More precisely, we believe that the following statement is true.

Conjecture 1 (RA-conjecture) *If conditions* (7) *and* (8) *are fulfilled at the codimension-2 point (when system $F_{\mu,\nu}$ has a homoclinic butterfly with a neutral saddle), then in the (μ,ν)-parameter plane there exists a nowhere dense closed set of positive Lebesgue measure which corresponds to the existence of the Rovella attractor, and the point $(\mu,\nu) = (0,1)$ belongs to its boundary.*

For the case $|A| > 2$, with additional restrictions on the eigenvalues of the saddle equilibrium, this statement was proved in Ref. [26]. In our forthcoming paper[52] we prove it for $|A| > 1$.

B. On the structure of periodicity windows in the RA-region: from the Lorenz attractor to the Rovella attractor

As mentioned above, in the RA-region there are no tangencies between the subspaces E^{ss} and E^{cu}. It implies that the stable and unstable invariant manifolds of periodic saddle orbits inside the Rovella attractor can intersect only transversally. Therefore, stable periodic orbits inside periodicity windows in RA cannot appear through bifurcations of homoclinic tangencies as it usually happens for quasiattractors. Here another mechanism of generation of periodicity windows is realized. This mechanism is illustrated by the bifurcation diagram presented in Figure 15.

Without loss of generality, let us consider the homoclinic bifurcation curve l_{12} (the corresponding homoclinic loop is shown in Fig. 10b). This curve intersects with the neutral saddle curve $l_{\nu=1}$ at the codimension-2 point LR_{12}. Like the point S, this point satisfies the conditions of Conjecture 1. Thus, above the corresponding periodicity window, the Rovella attractor originates from this point to the right of the curve $l_{\nu=1}$ according to the scenario proposed in Refs. [3] and [25], see also Fig. 5. As for the point S, the lower boundary of this periodicity window is formed by the curve t_{12} of a saddle-node bifurcation; a pair of newly born stable cycles degenerates into a homoclinic butterfly on the curve l_{12} and a symmetric cycle is born above this curve. Then, this cycle undergoes the pitchfork bifurcation on a curve p_{12}. A pair of asymmetric stable cycles, then, collides into a doubled (with respect to the homoclinic butterfly occurring on l_{12}) homoclinic butterfly on the curve l_{12}^2, an so on. After an infinite cascade of alternating homoclinic butterfly and pitchfork bifurcations the Rovella attractor is born above a curve l_{12}^{RA}.

Similar picture is observed also for other curves l_{1n}, as well as for multiround homoclinic curves existing between l_{1n} and l_{1n+1}. According to Afraimovich, Bykov, and L.P. Shilnikov[8], homoclinic butterfly bifurcations are dense inside the region with the Lorenz attractor. Apparently, these bifurcations are also dense in the line $l_{\nu=1}$. In order to confirm it we employ the so-called method of *kneading diagrams* proposed by A. Shilnikov[49,51,53,54].

We construct the kneading diagram using the following scheme. For given values of parameters we take one of the unstable separatrices of O, e.g. the right one Γ_2, and use it in order to obtain the kneading sequence $s_0, s_1, s_2, \ldots$ according to the following rule. If, on this separatrix, the first point in which the maximum of $|x|$ is positive ($x > 0$), then we assign $s_0 = 1$, else, if $x < 0$ at the first maximum of $|x|$, then we put $s_0 = 0$. Repeating this procedure, we assign s_j equal to 0 or 1 for $j = 1, \ldots, q$, where q is some predetermined integer number. Since we take the right separatrix Γ_2, the first symbol s_0 is always 1 and we take it out of the kneading sequence.

According to the Afraimovich-Bykov-Shilnikov geometric model[7,8] (see also Fig. 7), $s_j = 1$ means that the $(j+1)$-th point of intersection of the separatrix with Π lies in Π_2, and $s_j = 0$ means that this point lies in Π_1. If s_j changes for two close values of parameters, while symbols s_k with $k < j$ stay the same, it means that between these values of parameters there exist a value which corresponds to the existence of a j-round homoclinic loop.

For each kneading sequence $(s_1, s_2, \ldots, s_q)$ we compute the following sum $K = \sum_{i=1}^{q} s_i 2^{q-i}$. Note, K can take any integer value from 0 to $2^q - 1$ and two kneading sequences of the same length q are equal when the corresponding values of K are the same. Thus, in the parameter plane, boundaries between regions with different values of K correspond to homoclinic loops. In order to visualize these boundaries we paint regions with different K in different colors, employing the following color scheme[51]. The values of $K \in [0, (2^q - 1)/2)$ are

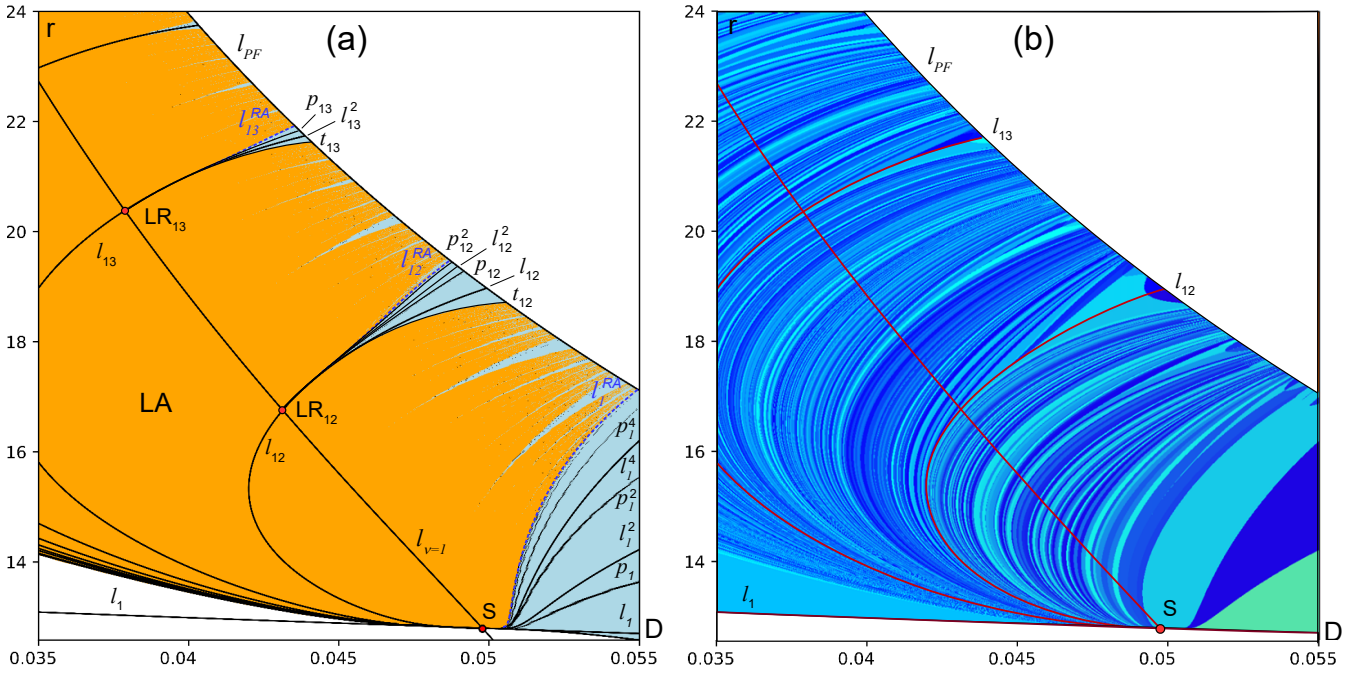

FIG. 15. (a) Bifurcation diagram illustrating the nature of periodicity windows inside the region RA: homoclinic bifurcation curves l^m_{1n} ($n = 2,3,\ldots$, $m = 2,3,\ldots$) correspond to the m-th doubling of the homoclinic loop occurring on l_{1n}; p^m_{1n} – supercritical pitchfork bifurcations of the symmetric stable cycle emerging from the corresponding homoclinic butterfly bifurcation; and (b) the corresponding kneading diagram illustrates, in particular, that homoclinic bifurcation points are dense on the curve $l_{\nu=1}$. Each such point (e.g. LR_{12} and LR_{13}) gives rise to the Rovella set (e.g. above the curves l^{RA}_{12} and l^{RA}_{13}) according to Conjecture 1.

converted to the depth of the red channel, while the blue channel has intensity 0. The values of $K \in [(2^q-1)/2, 2^q-1)]$ are converted to the depth of the blue channel, while the red channel has intensity 0. In both cases, the depth of the green channel is chosen randomly. We thank Andrey Shilnikov for clarifying these important technical details which help to obtain a contrasted picture.

The resulting graph – kneading diagram – is presented in Figure 15b. Here we take $q = 20$. In this figure, one can see that the family of homoclinic bifurcation curves forms a smooth foliation in the region LA.[55] It seems that this foliation is preserved on the curve $l_{\nu=1}$. This illustrates that homoclinic bifurcations are dense on this curve and the unfolding of each such bifurcation gives rise to the region of stability and the (multi-round) Rovella attractor above it.

V. ON THE BIRTH OF CHAOTIC ATTRACTORS AT CODIMENSION-2 BIFURCATION IN CASES: $0 < |A| < 1$, $1 < |A| < 2$, AND $|A| > 2$

In system (1) the cosimension-2 point S, where the homoclinic butterfly to the neutral saddle occurs, belongs to the boundaries of both the Lorenz attractor region and the region of Rovella attractor existence. Recall that $A \approx 1.19$ here, i.e., the case $1 < |A| < 2$ takes place. Two other cases of the organization of bifurcation diagram are possible when $0 < |A| < 1$ and $|A| > 2$. In order to illustrate it let us study the truncated factor map (3).

Figure 16 shows Lyapunov diagrams for map (3) when $A = 0.56$, $A = 1.19$, and $A = 2.2$ respectively. In these diagrams, lines $\mu = 0$ and l_2 correspond to the homoclinic and doubled homoclinic butterfly bifurcations, l_{het} and l_{het2} – heteroclinic bifurcations to saddle cycles. In the cases of Fig. 16a and Fig. 16b where $\nu < 1$, on l_{het}, the unstable separatrix Γ_1 (Γ_2) lie on the stable manifold of the saddle cycle C_2 (C_1); on the curve l_{het2}, Γ_1 (Γ_2) lies on the stable manifold of the two-round saddle cycle C_2^2 (C_1^2), respectively. Note that the cycles C_1 and C_2 are born from the homoclinic butterfly bifurcation on $\mu = 0$ and the cycles C_1^2 and C_2^2 are born below the curve l_2. In the cases of Fig. 16c and Fig. 16b where $\nu > 1$, on the curve l_{het}, the unstable separatices lie on the stable manifold of the symmetric pair of saddle cycles and above this curve almost all orbits tend to infinity in the case of three-dimensional system, after this bifurcation orbits tend to the stable equilibrium O_1 or O_2); on the curve l_{het2}, both unstable separatrices lies on the stable manifold of the the symmetric two-round saddle cycle S_0^2. Recall that after the birth (above the curve l_2), this cycle is stable and it becomes saddle via the supercritical pitchfork bifurcation. Note that Rovella proved the measure-persistence of chaotic attractors near such a type of bifurcation[4].

One can see that the boundaries of regions with chaotic dynamics near the point S depend on the mutual location of the curves l_{het}, l_2, and l_{het2}. Note that the first two curves for map (3) are defined by the following simple equations:

$$l_{het} : A\mu^{\nu-1} = 2,$$

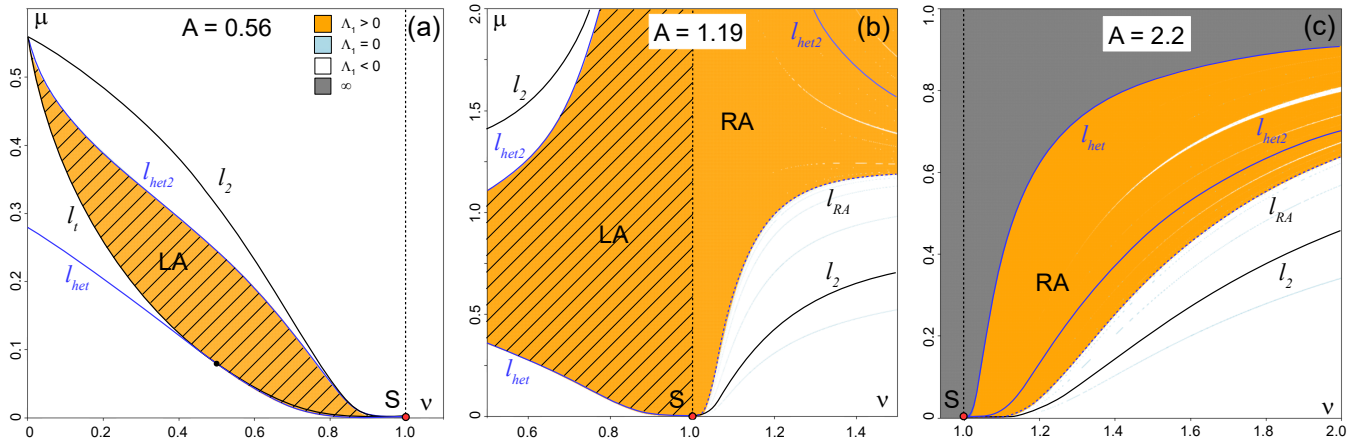

FIG. 16. Charts of the Lyapunov exponent and some bifurcation curves for map (3) for three principally different cases: (a) $A = 0.56$, the same as in the Shimizu-Morioka system (9), (b) $A = 1.19$, the same as in the Lyubimov-Zaks system (1), (c) $A = 2.2$ (examples of such systems are unknown). We use the same denotation for bifurcation curves as in Figs. 1; l_{het2} – heteroclinic bifurcation: the unstable separatrices lie on the stable manifold of a two-round saddle cycle. Dashed regions correspond to the existence of the Lorenz attractor. In the cases (a) and (b) $\nu < 1$, the pair of limit cycles (C_2^2 and C_1^2) is born below the doubled homoclinic butterfly bifurcation occurring on the curve l_2, while in the cases (c) and (b) $\nu > 1$, both separatrices lie on the stable manifold of the same symmetric saddle cycle S_0^2 (after the birth, above the curve l_2, this cycle is stable, it becomes saddle after the supercritical pitchfork bifurcation.

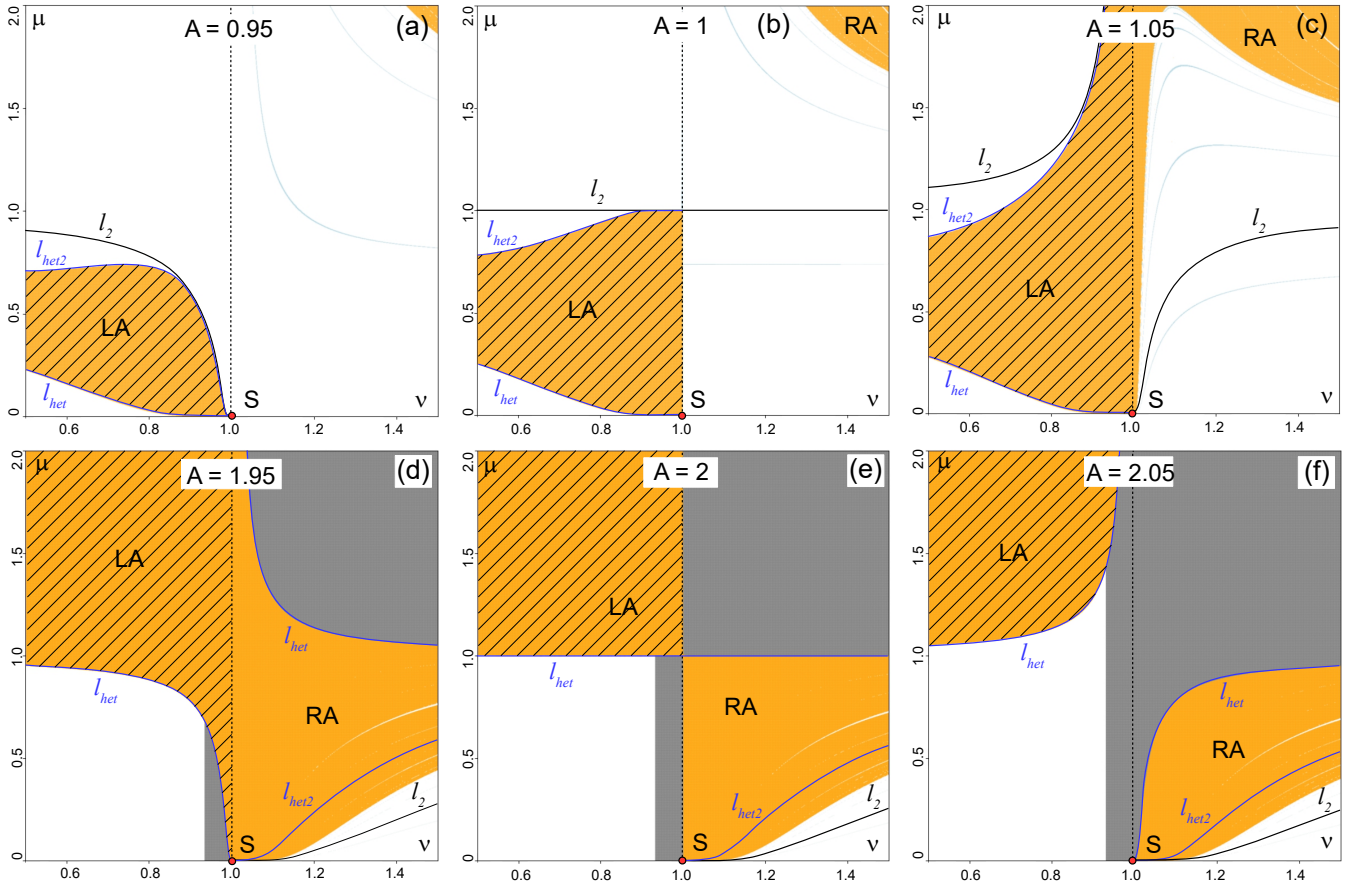

FIG. 17. Charts of the Lyapunov exponent and some bifurcation curves for map (3) near $A = 1$ (top row) and $A = 2$ (bottom row): (a) $A = 0.95$, (b) $A = 1$, (c) $A = 1.05$ (d) $A = 1.95$, (e) $A = 2$, and (f) $A = 2.05$. Here we use the same denotations for bifurcation curves as in Fig. 16.

and

$$l_2 : A\mu^{\nu-1} = 1.$$

In the case $0 < |A| < 1$, the curves l_{het} and l_{het2} originate from the point S and form the boundaries of the region LA of

the Lorenz attractor existence near this point. The situation changes drastically when $1 < |A| < 2$. Here, to the left of the line $\nu = 1$, l_2 and the curve l_{het2}, forming the upper boundary for the LA-region (near the point S), do not originate from the point S. They tend to infinity when $\nu \to 1$, and the curve $l_{\nu=1}$ also becomes the boundary of the region LA. Note that for such values of A, the doubled homoclinic bifurcation curve l_2 exists also to the right of the curve $\nu = 1$, where $\nu > 1$ (Fig. 16b), giving a possibility for the implementation of the scenario leading the Rovella-like chaotic attractors.

When $|A| > 2$, the curve l_{het} originates from the point S only where $\nu > 1$. Another segment of this curve, existing for $\nu < 1$, tends to infinity when $\nu \to 1$, see Fig. 17f. Thus, only the region RA with the Rovella-like attractors originates from the point S (see also Fig. 16c). Recall that the lower boundary of this region is formed by the limit curve l_{RA}. Alternating 2^n-round homoclinic and pitchfork bifurcation curves accumulate to this curve.

For a clearer explanation of the reconstruction of bifurcation curves near $A = 1$ and $A = 2$ we present six additional bifurcation diagrams in Figure 17. The upper three diagrams show the transition near $A = 1$ while the lower three diagrams explain the reconstruction of bifurcation curves near $A = 2$.

The described results can be summarized in the following statement. Depending on the absolute value of separatrix value A, three cases of the organization of bifurcation diagram near the point S (when the homoclinic butterfly to the neutral saddle equilibrium occurs) are possible:

1. when $0 < |A| < 1$, only a region of the existence of the Lorenz attractor adjoins to the point S, see Fig. 16a;
2. when $1 < |A| < 2$, both the Lorenz attractor region and the region of Rovella-like attractor existence adjoin to the point S, see Fig. 16b;
3. when $|A| > 2$, only the Rovella-like attractor region adjoins to the point S, see Fig. 16c.

A. Chaotic attractors in the Shimizu-Morioka model

Finally, based on the described above results, we would like to note and explain an interesting principal difference between the Lyubimov-Zaks system (1) and the well-known Shimizu-Morioka system

$$\begin{cases} \dot{x} = y \\ \dot{y} = x - \lambda y - xz \\ \dot{z} = -\alpha z + x^2. \end{cases} \tag{9}$$

for which the Shilnikov criterion is also applicable[9,14,16,17].

Figure 18 shows some bifurcation curves for system (9) superimposed with the Lyapunov diagram on the (α,λ)-parameter plane. This bifurcation diagram was obtained by A. Shilnikov[14–16]. Here we use the same denotations for bifurcation curves and points as for system (1), cf. Figs. 1 and 18. The homoclinic bifurcation curve l_1 intersects with the neutral saddle curve $l_{\nu=1}$ at the point S. The separatrix value in this point satisfies condition (4)[9,14,16]. Thus, according to the Shilnikov criterion, the Lorenz attractor existence region LA originates from this point. From one side, the same as in system (1), this region is bounded by the curve l_{het} where the unstable separatrices of O lie on the stable manifold of the saddle cycles. From the other side, the region LA is bounded by the curve l_{het2} on which the unstable separatrices lie on the stable manifold to the two-round saddle cycles which, in their turn, are born from the doubled homoclinic butterfly bifurcation (the curve l_2). We note, the curve l_{het2} is very close to l_2, therefore it is not plotted in Fig. 18. Also note that the region with chaotic dynamics entirely lies to the left of the curve $l_{\nu=1}$ where $\nu(O) > 1$, and the region with Rovella-like attractors does not exist to the right of this curve.

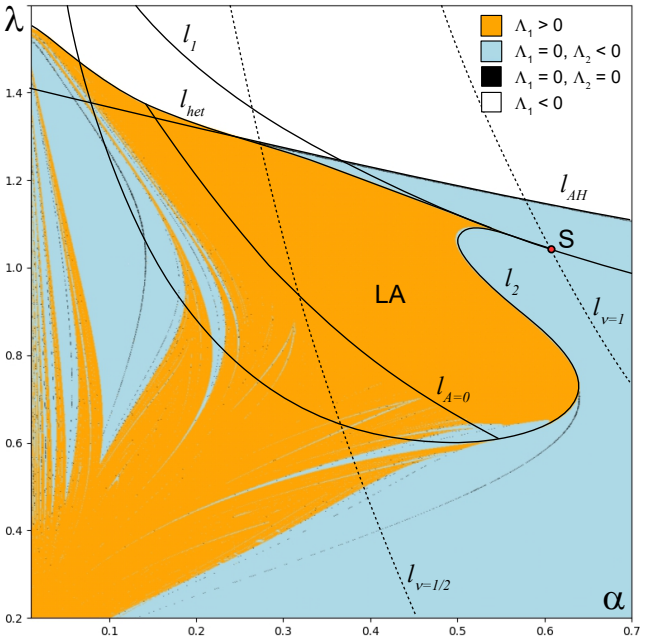

FIG. 18. Reproduction of the bifurcation diagram superimposed with the chart of Lyapunov exponents for the Shimizu-Morioka model (9). This diagram was obtained by A. Shilnikov[14–16]. For bifurcation curves and points we use here the same denotations as for system (1), see Fig. 1.

It is known that the separatrix value in system (9) satisfies the condition $0 < A < 1$[9,14,16,17]. Our numerics show that $A \approx 0.56$ here. The bifurcation diagram for the truncated factor map (3) in this case is shown in Fig. 16a. It explains why only a region with the Lorenz attractor originates from the point S.

Finally, we would like to note that bifurcation diagrams for the 1D map (3) and the 3D systems (1) and (9) are not completely equal. For example, since, for a fixed A, along the line $\nu = 1$, the truncated map is linear and, thus, it has a constant kneading, while in 3D systems the kneading sequence is changed along the neutral saddle-curve $l_{\nu=1}$. However, such changes also can be simulated by means of map (3) if to slightly modify it. For this goal, the separatrix value A should be considered not as a constant but as a slightly changing function depending e.g. on the parameter μ.

ACKNOWLEDGMENTS

The author thanks S. Gonchenko, K. Safonov, A. Shilnikov, and D. Turaev for fruitful discussions and useful remarks. Also the author is grateful to his students: A. Bobrovsky for help with Lyapunov diagrams, M. Kainov for help with pseudohyperbolicity verification, E. Karatetskaia for help with MatCont package, and S. Malykh for help with kneading diagram in Fig. 15b. The author also thanks anonymous reviewers for their careful reading and valuable comments.

This paper was supported by the RSF grant 19-71-10048. The results presented in Section V were obtained with the support of the Laboratory of Dynamical Systems and Applications NRU HSE, of the Ministry of science and higher education of the RF grant ag. № 075-15-2019-1931. Numerical experiments presented in Sec. IV were supported by the RBBR grant No. 18-29-10081 and by the Theoretical Physics and Mathematics Advancement Foundation "BASIS" grant No. 20-7-1-36-5.

DATA AVAILABILITY

The data supporting numerical experiments presented in this paper are available from the corresponding author upon reasonable request.

REFERENCES

[1]D. Turaev and L. P. Shilnikov, "An example of a wild strange attractor," Sbornik: Mathematics **189**, 291 (1998).
[2]D. Turaev and L. P. Shilnikov, "Pseudohyperbolicity and the problem on periodic perturbations of Lorenz-type attractors," Doklady Mathematics **77**, 17–21 (2008).
[3]D. Lyubimov and M. Zaks, "Two mechanisms of the transition to chaos in finite-dimensional models of convection," Physica D: Nonlinear Phenomena **9**, 52–64 (1983).
[4]A. Rovella, "The dynamics of perturbations of the contracting Lorenz attractor," Boletim da Sociedade Brasileira de Matemática-Bulletin/Brazilian Mathematical Society **24**, 233–259 (1993).
[5]L. Shilnikov, "The bifurcation theory and quasi-hyperbolic attractors," Uspehi Mat. Nauk **36**, 240–241 (1981).
[6]E. N. Lorenz, "Deterministic nonperiodic flow," Journal of atmospheric sciences **20**, 130–141 (1963).
[7]V. S. Afraimovich, V. Bykov, and L. P. Shilnikov, "On the origin and structure of the Lorenz attractor," Akademiia Nauk SSSR Doklady **234**, 336–339 (1977).
[8]V. S. Afraimovich, V. Bykov, and L. P. Shilnikov, "Attractive nonrough limit sets of Lorenz-attractor type," Trudy Moskovskoe Matematicheskoe Obshchestvo **44**, 150–212 (1982).
[9]M. J. Capiński, D. Turaev, and P. Zgliczyński, "Computer assisted proof of the existence of the Lorenz attractor in the Shimizu–Morioka system," Nonlinearity **31**, 5410 (2018).
[10]S. Gonchenko, A. Kazakov, and D. Turaev, "Wild pseudohyperbolic attractor in a four-dimensional Lorenz system," Nonlinearity **34**, 2018–2047 (2021).
[11]L. P. Shilnikov, A. Shilnikov, D. Turaev, and L. Chua, "Methods of qualitative theory in nonlinear dynamics. Parts I and II," World Scientific Series on Nonlinear Science, Series A **5** (1998,2001).
[12]C. Robinson, "Homoclinic bifurcation to a transitive attractor of Lorenz type," Nonlinearity **2**, 495 (1989).
[13]C. Robinson, "Homoclinic bifurcation to a transitive attractor of Lorenz type, ii," SIAM journal on mathematical analysis **23**, 1255–1268 (1992).
[14]A. Shilnikov, "Bifurcations and chaos in the Shimizu–Marioka system," in Methods and Qualitative Theory of Differential Equations, Gorky State University , 180–193 (1986).
[15]A. Shilnikov, "Bifurcation and chaos in the Morioka-Shimizu system," Selecta Math. Soviet **10**, 105–117 (1991).
[16]A. L. Shilnikov, "On bifurcations of the Lorenz attractor in the Shimizu-Morioka model," Physica D: Nonlinear Phenomena **62**, 338–346 (1993).
[17]A. L. Shilnikov, L. P. Shilnikov, and D. Turaev, "Normal forms and Lorenz attractors," International Journal of Bifurcation and Chaos **3**, 1123–1139 (1993).
[18]T. Shimizu and N. Morioka, "Chaos and limit cycles in the Lorenz model," Physics Letters A **66**, 182–184 (1978).
[19]G. Keller and M. S. Pierre, "Topological and measurable dynamics of Lorenz maps," in *Ergodic theory, analysis, and efficient simulation of dynamical systems* (Springer, 2001) pp. 333–361.
[20]V. Araújo, A. Castro, M. Pacifico, and V. Pinheiro, "Multidimensional Rovella-like attractors," Journal of Differential Equations **251**, 3163–3201 (2011).
[21]B. San Martín and K. Vivas, "The Rovella attractor is asymptotically sectional-hyperbolic," Nonlinearity **33**, 3036 (2020).
[22]M. V. Jakobson, "Absolutely continuous invariant measures for one-parameter families of one-dimensional maps," Communications in Mathematical Physics **81**, 39–88 (1981).
[23]M. Benedicks and L. Carleson, "On iterations of 1-ax2 on (-1, 1)," Annals of Mathematics , 1–25 (1985).
[24]M. Benedicks and L. Carleson, "The dynamics of the Hénon map," Annals of Mathematics **133**, 73–169 (1991).
[25]A. Arneodo, P. Coullet, and C. Tresser, "A possible new mechanism for the onset of turbulence," Physics Letters A **81**, 197–201 (1981).
[26]C. Morales, M. J. Pacifico, and B. S. Martin, "Contracting Lorenz attractors through resonant double homoclinic loops," SIAM journal on mathematical analysis **38**, 309–332 (2006).
[27]V. S. Afraimovich and L. P. Shilnikov, "Strange attractors and quasiattractors," (1983).
[28]P. V. Kuptsov, "Fast numerical test of hyperbolic chaos," Physical Review E **85**, 015203 (2012).
[29]P. V. Kuptsov and U. Parlitz, "Theory and computation of covariant Lyapunov vectors," Journal of nonlinear science **22**, 727–762 (2012).
[30]D. Turaev and L. P. Shilnikov, "Bifurcation of a homoclinic "figure eight" saddle with a negative saddle value," Doklady Akademii Nauk **290**, 1301–1304 (1986).
[31]M. Zaks and D. Lyubimov, "Bifurcation sequences in the dissipative systems with saddle equilibria," Banach Center Publications **1**, 367–380 (1989).
[32]M. A. Zaks, "Scaling properties and renormalization invariants for the "homoclinic quasiperiodicity"," Physica D: Nonlinear Phenomena **62**, 300–316 (1993).
[33]A. Dhooge, W. Govaerts, Y. A. Kuznetsov, H. G. E. Meijer, and B. Sautois, "New features of the software matcont for bifurcation analysis of dynamical systems," Mathematical and Computer Modelling of Dynamical Systems **14**, 147–175 (2008).
[34]V. De Witte, W. Govaerts, Y. A. Kuznetsov, and M. Friedman, "Interactive initialization and continuation of homoclinic and heteroclinic orbits in matlab," ACM Transactions on Mathematical Software (TOMS) **38**, 1–34 (2012).
[35]A. Bobrovsky, "Lyapunov plotter on python," (2021).
[36]G. Benettin, L. Galgani, A. Giorgilli, and J.-M. Strelcyn, "Lyapunov characteristic exponents for smooth dynamical systems and for Hamiltonian systems; a method for computing all of them. part 1: Theory," Meccanica **15**, 9–20 (1980).
[37]L. P. Shilnikov, "Bifurcation theory and the Lorenz model," Appendix to Russian edition of "The Hopf Bifurcation and Its Applications." Eds. J. Marsden and M. McCraken , 317–335 (1980).
[38]S. Gonchenko, Kainov, Kazakov, and D. Turaev, "On methods for verification of the pseudohyperbolicity of strange attractors," Izvestiya VUZ. Applied Nonlinear Dynamics **29**, 160–185 (2021).
[39]P. V. Kuptsov and A. Politi, "Large-deviation approach to space-time chaos," Physical review letters **107**, 114101 (2011).

[40]P. V. Kuptsov and S. P. Kuznetsov, "Lyapunov analysis of strange pseudohyperbolic attractors: angles between tangent subspaces, local volume expansion and contraction," Regular and Chaotic Dynamics **23**, 908–932 (2018).
[41]M. Malkin and K. Safonov, "Entropy charts and bifurcations for Lorenz maps with infinite derivatives," Chaos: An Interdisciplinary Journal of Nonlinear Science **31**, 043107 (2021), https://doi.org/10.1063/5.0040164.
[42]I. I. Ovsyannikov and D. Turaev, "Analytic proof of the existence of the Lorenz attractor in the extended Lorenz model," Nonlinearity **30**, 115 (2016).
[43]It is worth noting that inequality (4) in theorem 1 follows from equation (7) in Ref. [3].
[44]H. M. Osinga and B. Krauskopf, "Crocheting the Lorenz manifold," The Mathematical Intelligencer **26**, 25–37 (2004).
[45]E. J. Doedel, B. Krauskopf, and H. M. Osinga, "Global bifurcations of the Lorenz manifold," Nonlinearity **19**, 2947 (2006).
[46]J. L. Creaser, B. Krauskopf, and H. M. Osinga, "Finding first foliation tangencies in the Lorenz system," SIAM Journal on Applied Dynamical Systems **16**, 2127–2164 (2017).
[47]V. Bykov and A. Shilnikov, "On the boundaries of the domain of existence of the Lorenz attractor," Methods of Qualitative Theory and Theory of Bifurcations. Gorky State University, Gorky , 151–159 (1989).
[48]V. Bykov and A. Shilnikov, "On the boundaries of the domain of existence of the Lorenz attractor," Selecta Mathematica Sovietica **1**, 375–382 (1992).
[49]R. Barrio, A. Shilnikov, and L. Shilnikov, "Kneadings, symbolic dynamics and painting Lorenz chaos," International Journal of Bifurcation and Chaos **22**, 1230016 (2012).
[50]A. Shilnikov, "Bifurcations and chaos in the Shimizu–Morioka system: Ii," in Methods and Qualitative Theory of Differential Equations, Gorky State University , 130–137 (1989).
[51]T. Xing, R. Barrio, and A. Shilnikov, "Symbolic quest into homoclinic chaos," International Journal of Bifurcation and Chaos **24**, 1440004 (2014).
[52]A. Kazakov, M. Malkin, and K. Safonov, "Rovella attractors through a homoclinic butterfly bifurcation with a neutral saddle equilibrium," Regular and Chaotic Dynamics **in preparation** (2021).
[53]K. Pusuluri and A. Shilnikov, "Homoclinic chaos and its organization in a nonlinear optics model," Physical Review E **98**, 040202 (2018).
[54]K. Pusuluri, H. G. E. Meijer, and A. Shilnikov, "Homoclinic puzzles and chaos in a nonlinear laser model," Communications in Nonlinear Science and Numerical Simulation **93**, 105503 (2021).
[55]Such organization of the bifurcation diagram is related to the fact that the kneading sequence is the topological invariant for the Lorenz attractor[56,57].
[56]M. Malkin, "Rotation intervals and dynamics of lorenz-like maps," book Methods of qualitative theory of diff. eq., Gorki , 122–139 (1985).
[57]M.-C. Li and M. Malkin, "Smooth symmetric and lorenz models for unimodal maps," International Journal of Bifurcation and Chaos **13**, 3353–3371 (2003).